Article

Cell Reports

Critical Modulation of Hematopoietic Lineage Fate by Hepatic Leukemia Factor

Graphical Abstract

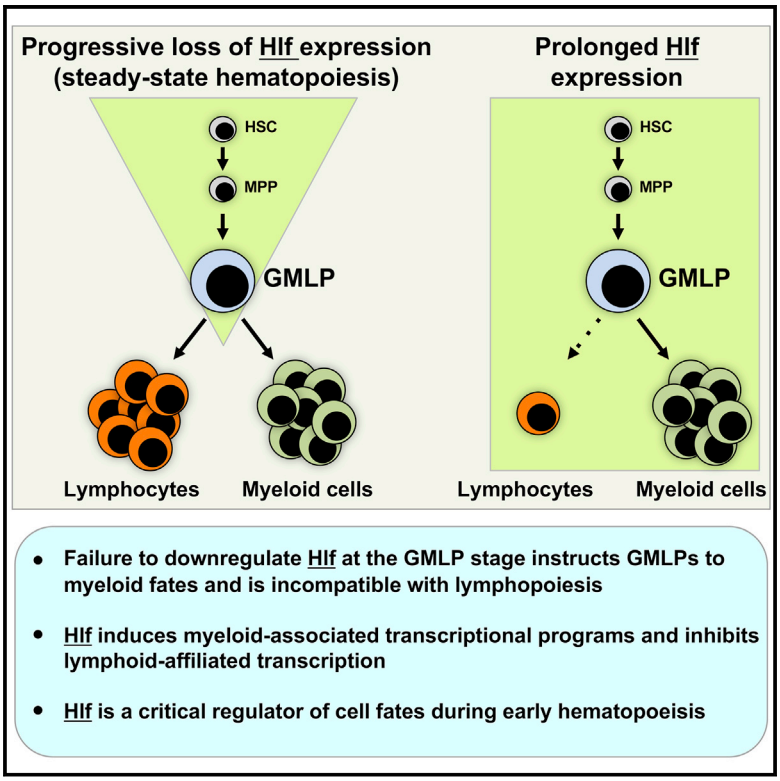

Authors

Martin Wahlestedt, Vasileios Ladopoulos, Isabel Hidalgo, ..., Gudmundur L. Norddahl, Berthold Göttgens, David Bryder

Correspondence

david.bryder@med.lu.se

In Brief

Regulators of early blood cell formation are important in both health and disease. Wahlestedt et al. identify abrupt downregulation of the transcription factor Hlf during hematopoietic differentiation. Failure to downregulate Hlf leads to a drastically skewed output of mature blood cells, positioning Hlf as a critical regulator of hematopoiesis.

Highlights

- During hematopoiesis, Hlf is sharply downregulated upon exit from multipotency
- Prolonged Hlf expression instructs GMLPs to adopt myeloid fates
- Failure to downregulate Hlf is incompatible with appropriate B and T lymphopoiesis
- Hlf governs molecular programs driving myelopoiesis and inhibiting lymphopoiesis

Data and Software Availability

GSE44923
GSE27686
GSE8407
GSE18734
GSE14833
GSE69817
GSE69858

Wahlestedt et al., 2017, Cell Reports *21*, 2251–2263
November 21, 2017
https://doi.org/10.1016/j.celrep.2017.10.112

Cell Reports
Article

Critical Modulation of Hematopoietic Lineage Fate by Hepatic Leukemia Factor

Martin Wahlestedt,[1] Vasileios Ladopoulos,[2] Isabel Hidalgo,[1] Manuel Sanchez Castillo,[2] Rebecca Hannah,[2] Petter Säwén,[1] Haixia Wan,[1] Monika Dudenhöffer-Pfeifer,[1] Mattias Magnusson,[3] Gudmundur L. Norddahl,[1] Berthold Göttgens,[2] and David Bryder[1,4,5,*]

[1]Lund University, Medical Faculty, Institution for Laboratory Medicine, Division of Molecular Hematology, Klinikgatan 26, BMC B12, 221 84 Lund, Sweden
[2]Department of Haematology, Wellcome Trust and MRC Cambridge Stem Cell Institute, Cambridge Institute for Medical Research, Cambridge University, Hills Road, Cambridge CB2 0XY, UK
[3]Lund University, Lund Stem Cell Center, Molecular Medicine and Gene Therapy, Sölvegatan 17, 221 84 Lund, Sweden
[4]StemTherapy, Lund University, 221 84 Lund, Sweden
[5]Lead Contact
*Correspondence: david.bryder@med.lu.se
https://doi.org/10.1016/j.celrep.2017.10.112

SUMMARY

A gradual restriction in lineage potential of multipotent stem/progenitor cells is a hallmark of adult hematopoiesis, but the underlying molecular events governing these processes remain incompletely understood. Here, we identified robust expression of the leukemia-associated transcription factor hepatic leukemia factor (Hlf) in normal multipotent hematopoietic progenitors, which was rapidly downregulated upon differentiation. Interference with its normal downregulation revealed Hlf as a strong negative regulator of lymphoid development, while remaining compatible with myeloid fates. Reciprocally, we observed rapid lymphoid commitment upon reduced Hlf activity. The arising phenotypes resulted from Hlf binding to active enhancers of myeloid-competent cells, transcriptional induction of myeloid, and ablation of lymphoid gene programs, with Hlf induction of nuclear factor I C (Nfic) as a functionally relevant target gene. Thereby, our studies establish Hlf as a key regulator of the earliest lineage-commitment events at the transition from multipotency to lineage-restricted progeny, with implications for both normal and malignant hematopoiesis.

INTRODUCTION

Blood cell formation is often viewed in a hierarchical manner, in which hematopoietic stem cells (HSCs) reside at the apex of the hematopoietic hierarchy (Figure 1A). Upon differentiation, HSCs produce intermediate progenitors with increasingly restricted lineage potential (Figure 1A). Although the extensive self-renewal that characterizes HSCs is lost in the initial stages of HSC differentiation, most existing data suggest that multipotency is retained. Thereafter, progenitors gradually lose multipotency through a branched differentiation scheme. Eventually, progenitors become locked to only one lineage, after which lineage-specific maturation events commence (Bryder et al., 2006; Mercer et al., 2011).

The lymphoid lineages (B, T and natural killer [NK] cells) branch from a common lymphoid progenitor (CLP) (Kondo et al., 1997). The generation of CLPs from upstream multipotent progenitors involves upregulation of lymphoid specification factors, such as Tcf3, Gfi-1, and Ikaros (Mercer et al., 2011). CLPs give rise to committed B cell progenitors, a process guided by a network of transcription factors (TFs) that includes Foxo1, Ebf1, and Pax5 (Mercer et al., 2011). Following initial maturation in the bone marrow (BM), immature B cells home to secondary hematopoietic organs for further maturation (Hardy and Hayakawa, 2001). T cells represent the other major lineage of lymphopoiesis. Although a matter of dispute, much data support that the earliest T cell progenitors (ETPs) can be generated from CLPs, although alternative parental progenitors might also exist (Allman et al., 2003; Benz et al., 2008; Kondo et al., 1997; Yang et al., 2010). Regardless, alternative lineage options of ETPs can be overridden by Notch signaling in the thymus, which acts by locking cells to the T cell lineage (Yang et al., 2010). In the thymus, ETPs mature through a series of immature progenitor stages (DN1–DN4) to eventually give rise to more mature T cells that are exported from the thymus (Germain, 2002). Myelopoiesis (giving rise to granulocytes, macrophages, erythroid cells, and platelets) represents the other dominant branch of hematopoiesis. Work from others and us has provided insight into the first stages of specification for these lineages (Akashi et al., 2000; Pronk et al., 2007). For instance, granulocyte/monocyte/lymphoid progenitors (GMLPs) retain a combined lymphoid and granulocyte/monocyte potential but harbor little or no erythroid (E) or megakaryocytic (Meg) potential (Adolfsson et al., 2005; Arinobu et al., 2007). Instead, the Meg and erythroid lineages are generated from a common pre-MegE progenitor, whose closest upstream progenitors remain a matter of debate (Adolfsson et al., 2005; Arinobu et al., 2007; Forsberg et al., 2006; Pronk et al., 2007; Sanjuan-Pla et al., 2013; Yamamoto et al., 2013).

Previously, we established the genome-wide expression patterns of highly purified HSCs and a range of defined

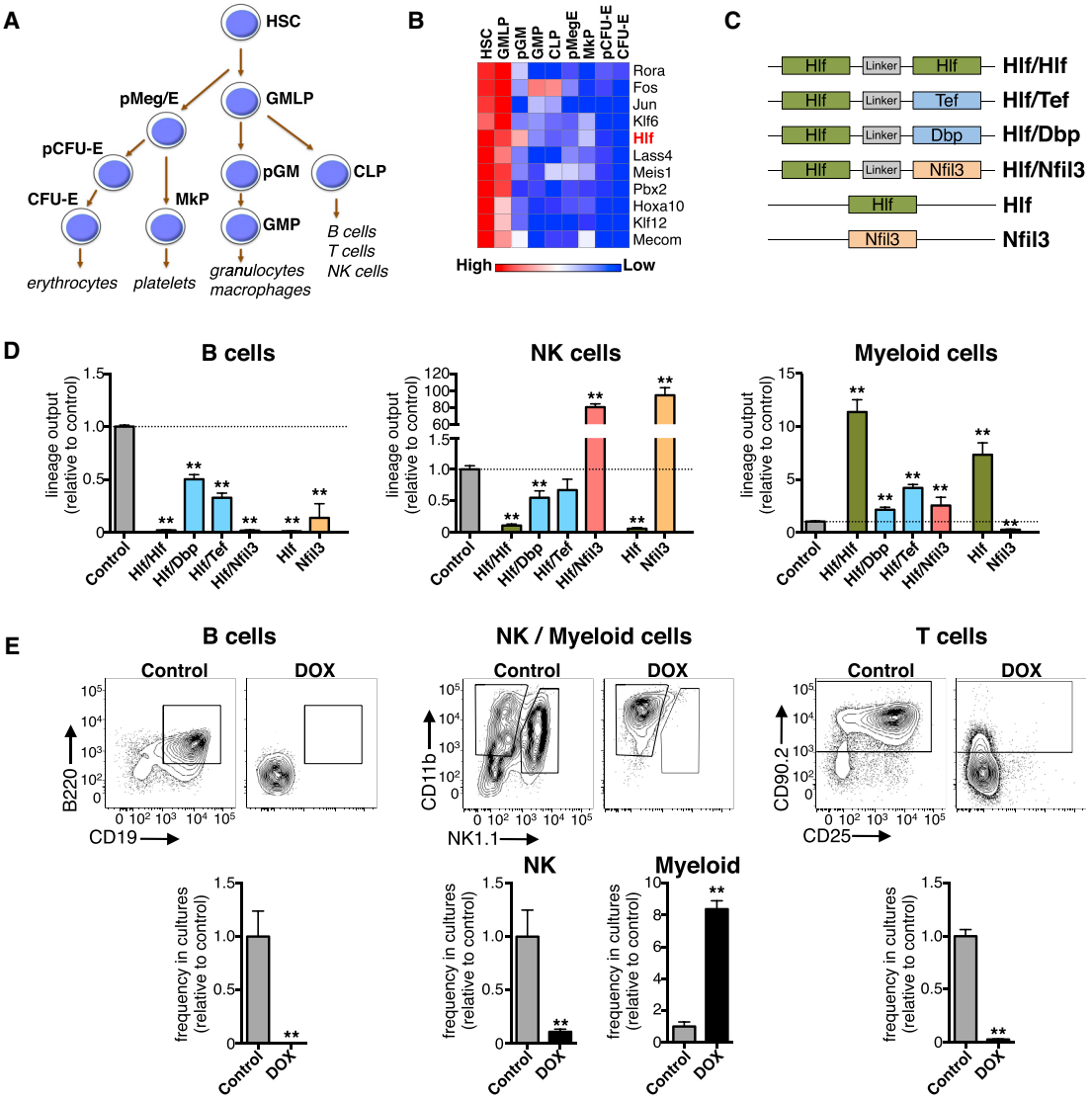

Figure 1. Identification of Hlf as a Candidate Regulator of Early Hematopoiesis

(A) Schematic depiction of the progenitor subsets that underlie the early stages of hematopoiesis.

(B) Heatmap showing the expression levels of TFs displaying 2-fold or higher expression in HSCs and GMLPs compared with downstream progenitor cell types (mean values of three replicate arrays per cell type, except for HSCs and pMegEs, for which six and five replicate arrays were used, respectively). See also Table S1.

(C) Schematic depiction of the different lentiviral constructs used for OP9 stromal co-cultures.

(D) The lineage output relative to controls of B cells, NK cells, and myeloid cells produced from Hlf/Hlf, Hlf/Dbp, Hlf/Tef, Hlf/Nfil3, Hlf, Nfil3, and M33-Hlf transduced GMLPs in OP9 stroma co-cultures (n = 6, 6, 6, 6, 6, 3, 6, and 45 cultures, respectively, from two independent experiments).

(E) B, NK, and myeloid cell generation in OP9 co-culture experiments and T cell generation in OP9-DL1 co-cultures using Hlf-inducible GMLPs cultured in the absence or presence of DOX. Shown are representative FACS plots as well as bar graphs showing the frequency relative to untreated controls of $CD19^+$ B cells, $NK1.1^+$ NK cells, $CD11b^+$ myeloid cells, and $CD90^+$ T cells in the cultures from three independent experiments (n = 5 for the B, NK, and myeloid experiments, and n = 9 for the T cell experiments).

Error bars denote SEM. CFU-erythroid, colony-forming unit-erythroid; MkP, megakaryocyte progenitor; pCFU-erythroid, pre-colony-forming unit-erythroid; pGM, pre-granulocyte-monocyte progenitor; pMeg/erythroid, pre-megakaryocyte-erythroid progenitor. See also Figures S1 and S2.

hematopoietic progenitor subsets (Norddahl et al., 2011; Pronk et al., 2007, 2008; Wahlestedt et al., 2013; Weishaupt et al., 2010; Figure 1A). When interrogating these datasets for expression of TFs that associate with multipotency and rapid down-regulation with differentiation (Figures 1B, S1, and S2), we identified hepatic leukemia factor (Hlf), a TF of the proline and acidic amino acid-rich basic leucine zipper family, previously studied for its role in circadian rhythm regulated neurotransmitter metabolism in the brain (Gachon et al., 2004; Mitsui et al., 2001), xenobiotic detoxification in the liver (Gachon et al., 2006), and

renal function (Zuber et al., 2009). Although Hlf was originally proposed to not be expressed in BM (Inukai et al., 2005), later studies found its promoter differentially methylated in between multipotent progenitor cells and more committed cells (Ji et al., 2010), with enforced expression of Hlf linked to enhanced self-renewal (Gazit et al., 2013; Shojaei et al., 2005). More recently, Hlf was identified as a necessary factor to revert committed blood cells back into an HSC-like state (Riddell et al., 2014). Hlf has perhaps a more well established connection to leukemia as the fusion partner of TCF3/E2A resulting from the t(17;19) translocation, a rare but recurrent event associated with a highly aggressive subset of acute B-lymphoblastic leukemia (Fischer et al., 2015; Hunger et al., 1992; Inaba et al., 1992). However, little is known on how Hlf might influence on normal hematopoietic differentiation. Therefore, we set out to characterize the role of Hlf in normal hematopoietic lineage development.

RESULTS

Prolonged Hlf Expression Critically Influences Multilineage Hematopoietic Differentiation

To begin to dissect the impact of Hlf on hematopoietic development, we first generated lentiviral constructs that included a single-copy Hlf overexpression vector and a construct in which Hlf is expressed as a forced homodimer (Hlf/Hlf; Figure 1C). We chose this complementary approach because HLH TFs generally target DNA as dimers. Although expression data suggested that Hlf is the only PAR bZIP family member with selectively high expression in immature blood cells, Hlf may affect early hematopoiesis by heterodimerizing with any of its other family members upon differentiation. We therefore also generated Hlf/Dbp, Hlf/Nfil3, and Hlf/Tef forced dimer constructs (Figure 1C) along with an Nfil3 overexpression vector, the latter because Nfil3 has been reported to act antagonistically to Hlf (Mitsui et al., 2001).

After confirmation of relevant Hlf expression induced by the different viral constructs (Figure S3A), transduced multipotent GMLPs were assessed using the OP9 stromal cell system (Nakano et al., 1994). These experiments revealed that Hlf and Hlf/Hlf overexpressing GMLPs displayed a strikingly reduced capacity to differentiate into $CD19^+$ B cells and $NK1.1^+$ NK cells, but with enhanced generation of $Gr\text{-}1^+/CD11b^+$ myeloid (Figure 1D). Overexpression of Nfil3 led to almost exclusive differentiation into NK cells (Figure 1D), reinforcing the importance of Nfil3 for NK cell development (Kamizono et al., 2009). A similar increase in NK cell development was observed from cells transduced with the Hlf/Nfil3 heterodimer construct (Figure 1D), suggesting that Nfil3 acts dominantly over Hlf. Finally, Hlf/Dbp and Hlf/Tef presented with an intermediate reduction in B and NK cell differentiation and an increase in myelopoiesis (Figure 1D).

To obtain a more controllable transgenic system, we next established a Tet-ON mouse model that upon doxycycline (DOX) administration allows conditional expression of Hlf (Figure S3B). Although systemic administration of DOX in these mice results in ubiquitous induction of transgene expression, its combination with cell isolation allows inducible expression of Hlf in any cell type of choice. To verify this model, we isolated Hlf-inducible GMLPs and subjected them to the OP9 co-culture system. In addition, we also investigated T lymphopoiesis by culturing transgenic GMLPs on OP9-DL1 stromal cells (Schmitt and Zúñiga-Pflücker, 2002). These experiments confirmed our previous findings using lentiviral-mediated transgenesis (Figure 1E), and OP9-DL1 co-culture experiments revealed that a failure to downregulate Hlf also inhibited T cell development (Figure 1E).

In Vivo Induction of Hlf Associates with Enhanced Myelopoiesis and Repressed Lymphopoiesis

To investigate the roles of Hlf *in vivo*, we provided Hlf-inducible mice with DOX via their food. Analyses of BM from these mice revealed a slight but significant reduction in overall cellularity as early as 3 days following Hlf induction (Figure S4A). To investigate hematopoiesis in detail, we enumerated multipotent cell compartments (HSCs and GMLPs), early myeloid precursors, and different stages of B cell development (Figure S4B and Table S1). HSC numbers in the BM of Hlf-induced mice were mildly increased at 3 days and decreased at 14 days of Hlf induction (Figure 2A). GMLPs were unaltered at all time points except following 11 days of Hlf induction, when a slight decrease in their numbers was observed (Figure 2A). By contrast, we observed a robust and progressive increase of pre-granulocyte-monocyte progenitors (pGMs) and granulocyte-monocyte progenitors (GMPs) over time (Figure 2A). Investigations into early lymphoid development in the BM revealed a slightly decreased abundance of B cell-biased lymphoid progenitors (BLPs) (Inlay et al., 2009) (Figure 2A). A more dramatic depletion was observed in downstream B lymphocyte precursor populations, including Hardy's fractions A, B-C, C′-D, and E (Hardy et al., 1991; Tung et al., 2004) (Figure 2B). By contrast, fraction F cells (mature recirculating B cells) (Hardy et al., 1991; Tung et al., 2004) were less affected (Figure 2B). These observations were accompanied by marked increases of a BM cell population with a $Lin^-B220^+CD19^+CD24^+IgM^-IgD^-c\text{-}Kit^+IL7Ra^+$ phenotype (Figure 2B). Retention of CD19 expression *in vitro* when cultured on both OP9 and OP9-DL1 stroma (data not shown), expression of several B cell-associated genes at levels comparable with fraction B-C cells, varying degrees of DJ and VDJ heavy-chain rearrangements, and their cell surface marker profile strongly suggested that they indeed represented a subset of early B cell progenitors (Figure S5). When Hlf was induced in fraction B-C cells for 48 hr, a large fraction of the cells ($31.5 \pm 8.1\%$, as opposed to $10.4 \pm 3.6\%$ of control cells) upregulated c-kit expression (Figure S4E), further emphasizing that the differentiation block in the B cell lineage caused by Hlf associates with a rapid induction of c-kit expression. In the spleen, the frequency of immature B cells was progressively decreased upon Hlf induction, whereas mature follicular B cells and marginal zone B cells were less affected (Figure 2B). The negative impact of Hlf on B lymphopoiesis therefore starts early and affects multiple progenitor stages, with little or no impact on more mature B cells.

We next asked whether Hlf might affect T cell development *in vivo*. Surprisingly, as early as 3 days after initiation of Hlf expression, we observed pronounced thymic atrophy that

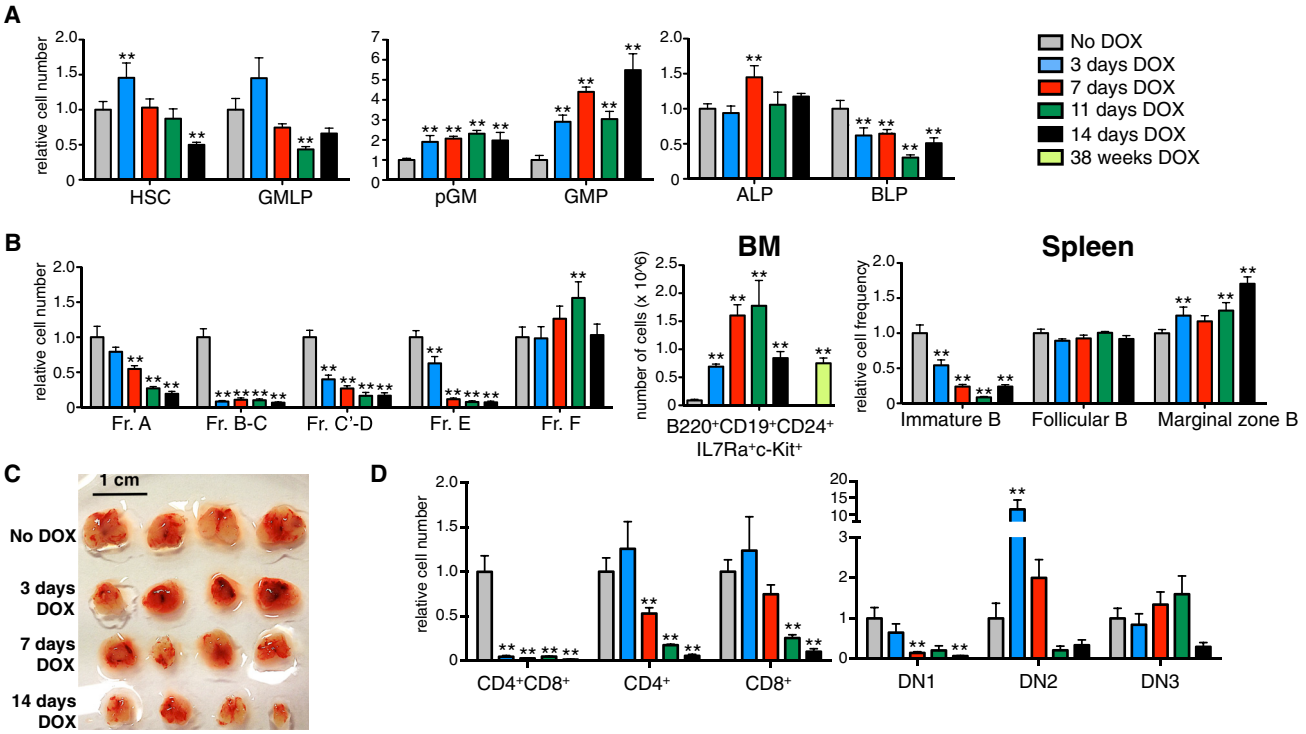

Figure 2. Hlf Induction *In Vivo* Negatively Influences Lymphopoiesis at the Expense of Enhanced Myelopoiesis

Hlf-inducible mice were given DOX via their food pellets for 0, 3, 7, 11, and 14 days (n = 7, 7, 7, 3, and 4 mice in each group, respectively, from two independent experiments) and 38 weeks (n = 5 mice, from one experiment).

(A) Bar charts showing the amount of HSCs, GMLPs, pGMs, GMPs, all lymphoid progenitors (ALPs), and B cell-biased lymphoid progenitors (BLPs) in the BM of the analyzed mice (relative to uninduced mice).

(B) Relative cell numbers of the analyzed B cell subsets in the BM and relative frequencies of the indicated splenic B cell fractions among all splenocytes in the analyzed mice (relative to uninduced mice). See also Figure S5.

(C) Photographs depicting thymi after 0, 3, 7, 11, and 14 days of enforced Hlf expression (four thymi per time point, representative of one of three experiments). The scale bar represents 1 cm.

(D) The amount of $CD4^+CD8^+$ double-positive, single-positive $CD4^+$, single-positive $CD8^+$ thymocytes, and DN1, DN2, and DN3 thymocytes following the different number of days of DOX administration (relative to uninduced mice). See also Table S1.

Error bars denote SEM. ALP, all lymphoid progenitor; BM, bone marrow; BLP, B cell biased lymphoid progenitor; DN, double negative. See also Figures S3 and S4.

progressed rapidly (Figure 2C). Reasoning that this might be connected to thymic T cell development, we enumerated different T cell compartments (Figure S4C). After 3 days, $CD4^+$ and $CD8^+$ single-positive T cells were present at normal numbers, whereas $CD4^+CD8^+$ double-positive T cell numbers were dramatically decreased (Figure 2D). Analysis of $CD4^+CD8^+$ cells following brief Hlf induction *in vitro* revealed a massive induction of apoptosis (Figure S4D). Upon longer Hlf induction, the decrease in $CD4^+CD8^+$ cells persisted and single-positive subsets gradually decreased in numbers, such that by day 14, levels were only 5.7% ($CD4^+$) and 10.2% ($CD8^+$) of those observed in control mice (Figure 2D). When investigating more primitive T cell fractions, we observed a pronounced decrease in double-negative (DN) 1 cells (Figure 2D) from day 7 onward. DN2 cells were greatly expanded following 3 days of induction (~7-fold; Figure 2D). However, this was attenuated 4 days later, and at 11 and 14 days, their levels displayed a decreasing trend compared with control mice (Figure 2D). Last, DN3 cells were present at normal numbers up to 11 days following Hlf induction but decreased by day 14 and at later time points (Figure 2D and data not shown).

Hlf Acts Intrinsically on Hematopoiesis

To exclude the possibility that Hlf mediates an indirect effect, we next transplanted Hlf-inducible GMLPs into sublethally irradiated wild-type (WT) mice under continuous Hlf induction. Twenty-one days post-transplantation, the Hlf-induced cells presented with a dramatic (28-fold) increase in myeloid cell reconstitution in the BM (Figure 3A). Somewhat surprisingly, we observed that $CD19^+$ BM B cell reconstitution was increased 12-fold over the control (Figure 3A). More detailed examination revealed that these cells were almost exclusively restricted to the aforementioned population with a $Lin^-B220^+CD19^+c\text{-}Kit^+IL7Ra^+$ phenotype (Figure 3B). Despite the dramatic expansion of this subset in the BM, B cell reconstitution was dramatically reduced in the spleen (3.4-fold) (Figure 3C) and in peripheral blood (PB) (5.7-fold) (Figure 3D). In agreement with the increased myeloid reconstitution in the BM, donor-derived myeloid cell abundance

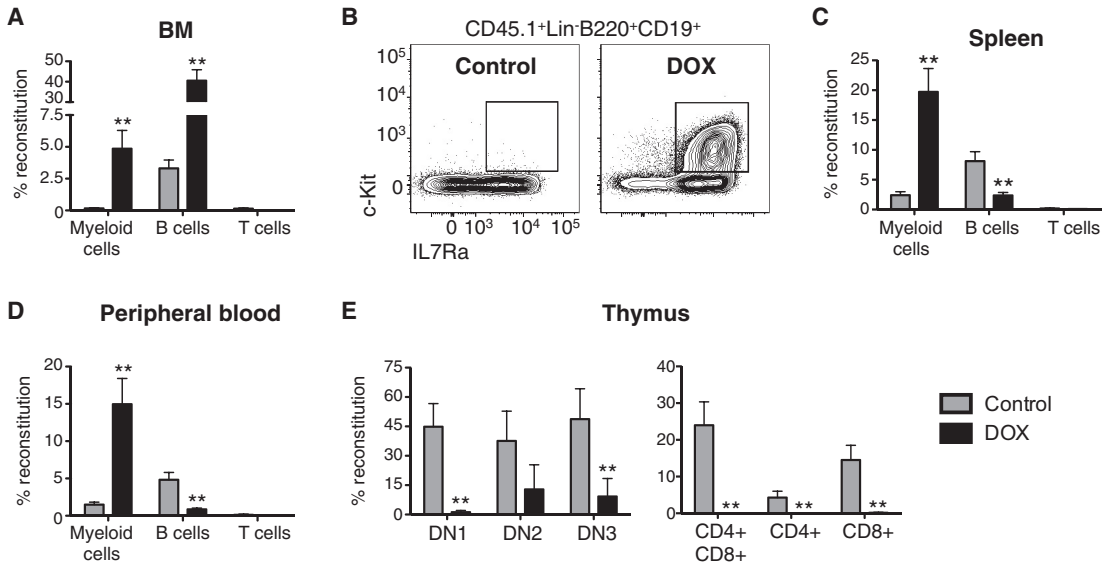

Figure 3. Cell-Autonomous Alterations Underlie the Altered Hematopoiesis Following Enforced Hlf Expression *In Vivo*

Hlf-inducible GMLPs (CD45.1$^+$) were transplanted into sublethally irradiated WT recipient hosts (CD45.2$^+$) maintained on a DOX food diet (n = 6 and 7 mice for the control and DOX groups, respectively, from one of three experiments with similar results).

(A) Magnitudes of myeloid B, and T cell reconstitution in the BM of the recipient mice.

(B) FACS plots showing the appearance of CD45.1$^+$c-Kit$^+$IL7Ra$^+$CD19$^+$ cells in the BM of mice transplanted with Hlf-induced GMLPs.

(C and D) Donor-derived reconstitution of myeloid, B, and T cells in the spleen (C) and the PB (D).

(E) The thymi of recipient mice were assessed for donor-derived reconstitution of the indicated thymocyte subsets.

Error bars denote SEM. See also Figure S5.

was increased 8.3-fold and 10.1-fold in the spleen and PB, respectively (Figures 3C and 3D). In the thymus, Hlf induction led to a total absence of donor-derived CD4$^+$, CD8$^+$, or CD4$^+$CD8$^+$ cells (Figure 3E). Although reconstitution of the more primitive DN1–DN3 cells was significantly lower than from control cells, their presence in induced mice suggested that initial homing to the thymus was at least to some degree functional (Figure 3E).

Acute Loss and the Modulation of Hlf into a Transcriptional Repressor Enhance Lymphopoiesis from Multipotent Progenitors

Next, we approached the roles of Hlf from a loss-of-function perspective. Because Hlf is rapidly downregulated upon normal differentiation, traditional knockout experiments provide little information. Therefore, we first transplanted mice with Hlf transgenic GMLPs under Hlf induction for 14 days. This was followed by removal of Hlf induction for 8 days to reduce Hlf levels. Compared with cells with continuous Hlf expression, Hlf depletion resulted in a rapid shift in PB lineage distribution, owing to an 8.7-fold increase in B cells (Figure 4A). Similarly, although continuous Hlf expression failed to associate with splenic T cell reconstitution, we detected low but consistent T cell generation following Hlf withdrawal (Figure 4A). Investigations of the BM revealed that the otherwise vastly expanded Lin$^-$B220$^+$CD19$^+$c-Kit$^+$IL7Ra$^+$ population had greatly decreased in size (10.9-fold) following Hlf depletion, which coincided with strikingly elevated numbers at all stages of early B lymphopoiesis. Thus, the accumulation of this population represents a differentiation block that is released following DOX withdrawal (Figure 4A). In this setting, we failed to observe a decrease in myeloid cell output upon DOX withdrawal, which likely reflects the limited self-renewal potential of GMLPs and the fact that myeloid lineage commitment has already commenced during the induction period.

We next generated an M33-Hlf construct, in which the strong repressive domain of the polycomb gene M33 (Cbx2) is predicted to turn Hlf from a transcriptional activator into a repressor (Argiropoulos et al., 2010). We reasoned that such an approach was highly relevant, given that Hlf associated mostly with transcriptionally active genes (see below). We introduced the M33-Hlf construct into WT GMLPs and subjected cells to OP9 and OP9-DL1 differentiation conditions. In OP9 cultures, expression of M33-Hlf led to an increased production of B cells and NK cells, with little influence on myeloid cell generation (Figure 4B). In OP9-DL1 co-cultures, the overall T cell production from M33-Hlf expressing GMLPs was enhanced, mainly because of an increase of DN3 cells at the expense of DN1 and DN2 cells (Figure 4C).

The Genome-wide Binding Characteristics of Hlf

We were next interested in identifying the genomic regions occupied by Hlf. For this, we generated a retroviral vector expressing a FLAG-tagged variant of Hlf and used this to infect Lin$^-$Sca-1$^+$c-Kit$^+$ (LSK) cells. Although HSCs are included in the LSK fraction, the majority of cells in this population (>95%) represent multipotent progenitors (Bryder et al., 2006). Therefore, most observed binding represents Hlf activity in multipotent progenitors. Following 5 days of expansion, the infected cells

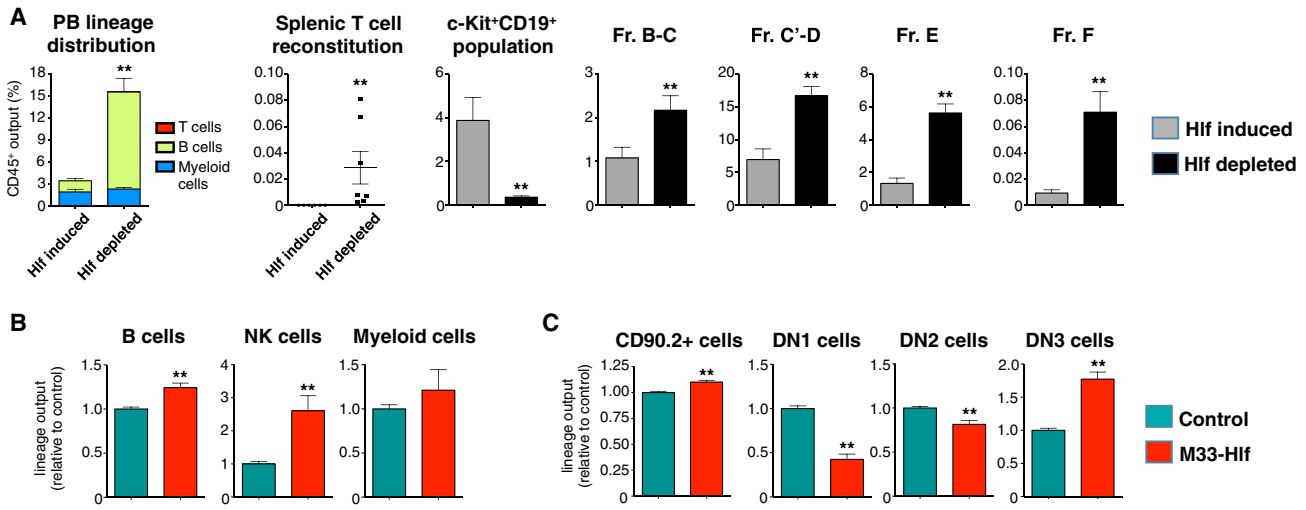

Figure 4. Acute Hlf Depletion and Modulation of Hlf into a Transcriptional Repressor Lead to Enhanced Lymphopoiesis

Hlf-inducible GMLPs (CD45.1$^+$) were transplanted into sublethally irradiated WT recipients (CD45.2$^+$) on DOX food. After 14 days, one group of mice was shifted to normal food and kept for another 8 days prior to analysis ("Hlf depleted"), while control mice were treated with DOX throughout the experiment ("Hlf induced," n = 7 and 6 mice, respectively, from one experiment).

(A) Data show the percentage of the indicated donor-derived cell types out of all CD45$^+$ cells.

(B and C) The impact of Hlf target gene silencing on differentiation was studied by culturing control or M33-Hlf retrovirus infected WT GMLPs in B/NK and T cell permissive conditions (n = 6 replicates per group from two experiments). Shown is the lineage output relative to controls of indicated subsets in OP9 cultures (B) and OP9-DL1 cultures (C), respectively.

Error bars denote SEM.

were next used for chromatin immunoprecipitation sequencing (ChIP-seq) analysis using anti-FLAG or control antibodies. This revealed Hlf peaks scattered around different genomic regions; 7.4% of the sites were located at promoters, 1.8% in UTR regions, 45% at intragenic sites, and 45.8% in intergenic regions (Figure S6A). Investigations into a putative underlying Hlf-binding motif of the peaks revealed a predicted motif closely resembling that reported for human HLF (Inaba et al., 1994) (Figure S6B). Overrepresented gene ontology categories and mouse phenotypes on the basis of the predicted Hlf-binding peaks associated with blood cell development or immune system processes, further supporting the notion of Hlf as a regulator of blood cell formation (Figure S6C).

To investigate whether the intergenic peaks might overlap with known enhancer regions, we intersected them with enhancer regions recently identified in a variety of hematopoietic cell types on the basis of H3K27Ac occupancy (Lara-Astiaso et al., 2014) (Figure 5A). The elements bound by Hlf associated with a random distribution of H3K27Ac in mature B and T cells. In contrast, in long-term HSCs (LT-HSCs), short-term HSCs (ST-HSCs), multipotent progenitor (MPP), common myeloid progenitor (CMP), GMP, mature granulocytes, and CLPs, Hlf peaks correlated with highly acetylated H3K27Ac positioned on either side of the Hlf peak summit, suggesting that Hlf may affect hematopoietic development by regulating transcription also via enhancer elements (Figure 5A). Further supporting this was the observation that identified binding motifs of several other well-known hematopoietic TFs, including c/EBP-like, Ets, Runx1, and AP1, co-associated with the identified Hlf peak areas (Figure S6D).

We thereafter compared the identified Hlf-bound regions with those of other hematopoietic TFs. This revealed a strong correlation between Hlf binding and c/EBP binding (Figure 5B), which has been proposed previously (Hunger et al., 1992), and suggested that Hlf might share c/EBP-binding sites during hematopoietic development. To functionally test a redundancy among these factors, we investigated if aberrant Hlf expression may lead to transdifferentiation of B cells into macrophages, as has previously been reported for C/EBP factors (Xie et al., 2004). However, although Cebpb efficiently transdifferentiated B cells into macrophages, Hlf was unable to do so (Figure 5C), demonstrating that although the underlying binding motif of Cebp and Hlf is similar, the functions of these factors are distinct.

Hlf Confers a Myeloid Fate on GMLPs that Is Accompanied by a Deregulation of Lymphoid and Myeloid Gene Expression Programs

Although our data suggested that Hlf acts as a strong lineage fate determinant in multipotent progenitors, it remained a possibility that one subset of GMLPs responded to Hlf by allowing enhanced myelopoiesis, while an alternative lymphoid-competent subset was selectively depleted. To investigate this, using fluorescence-activated cell sorting (FACS), we sorted individual Hlf-inducible GMLPs onto OP9 stromal cells under B and NK cell-promoting conditions and analyzed their progeny 14 days later. Forced Hlf induction significantly increased the cloning frequency (the ability of single-seeded GMLPs to promote growth of detectable progeny) by 50% (36.4% in the absence and 54.5% in the presence of DOX) (Figure S7A). WT GMLPs produced a variety of lineage outputs, in which lymphoid

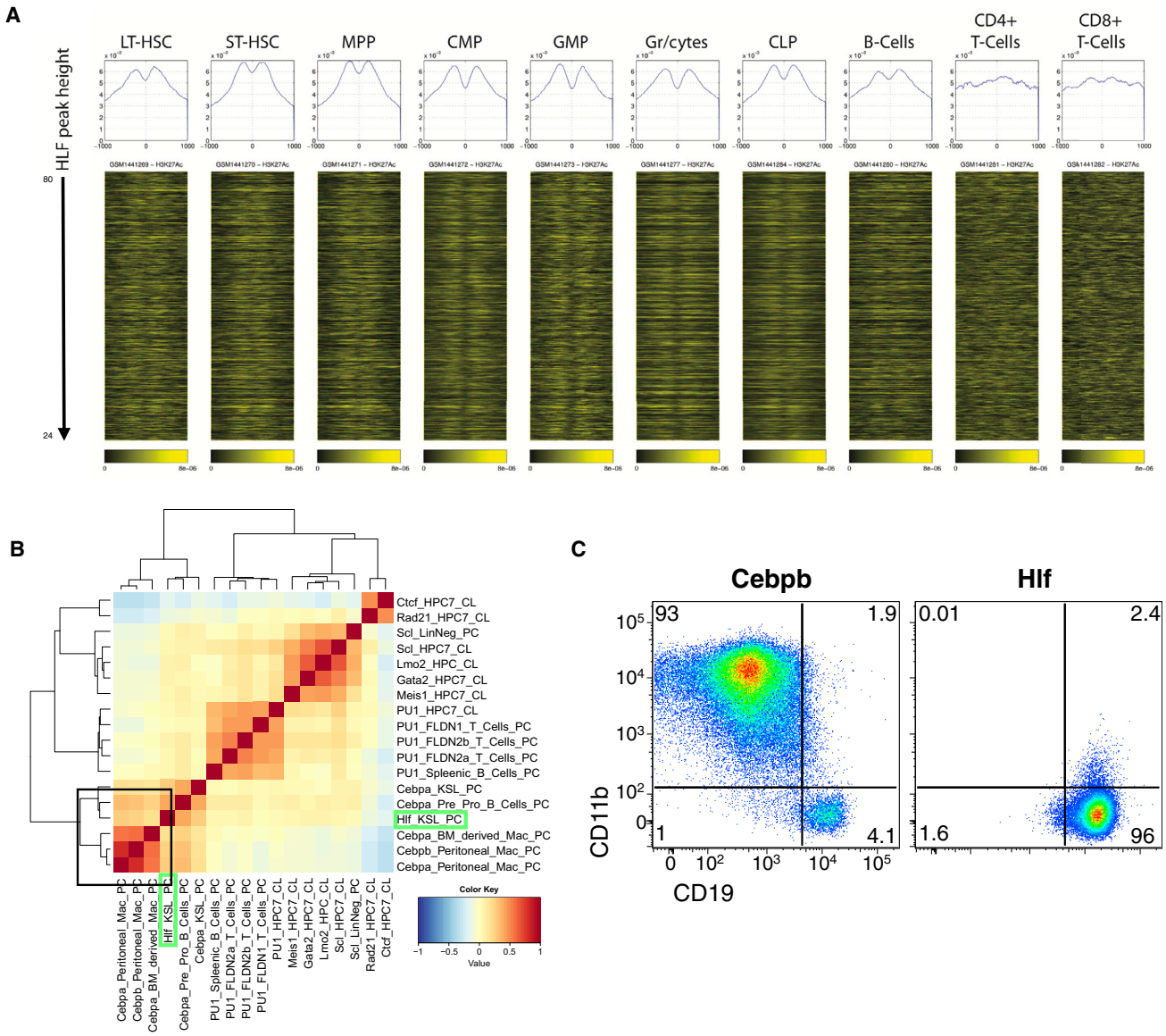

Figure 5. The Genome-wide Binding Characteristics of Hlf

WT LSK cells were transduced with either a control retroviral vector or a vector encoding an N-terminal FLAG-tagged variant of Hlf/Hlf and were subjected to ChIP-seq analysis.

(A) The Hlf peaks were ranked in a decreasing peak height order, and H3K27Ac signal intensity (Lara-Astiaso et al., 2014) was plotted around the summit of the Hlf peaks and is shown as heatmaps. The histograms at the top of each heatmap depict the average signal intensity around the Hlf peaks for each cell type.

(B) Correlation analysis of the putative Hlf targets with those of other hematopoiesis associated TFs.

(C) BM resident B cells were subjected to transdifferentiation experiments by transduction with retroviral vectors encoding Cebpb or Hlf and cultured for 4 days on OP9 stromal cells prior to FACS analysis (representative FACS plots from two independent experiments).

ChIP, chromatin immunoprecipitation. See also Figure S6.

potential was dominant (Figure 6A). In stark contrast, forced Hlf expression caused most cells (96.5%) to produce only myeloid progeny (Figure 6A). These data strongly suggested that Hlf acts to divert lineage fate of multipotent GMLPs, rather than exercising differential effects on already committed progenitors. To investigate the genome-wide transcriptional consequences underlying this, we next conducted RNA sequencing (RNA-seq). We here used both viral-mediated overexpression in WT GMLPs and GMLPs from our inducible transgenic mouse strain (Figure S7B). We chose to use these complementary approaches to try to overcome limitations associated with each individual approach. By highly stringent analysis criteria, this combinatory approach revealed 43 and 41 up- and downregulated genes as a consequence of Hlf expression, respectively (Figure 6B; Table S2). In general, the most differentially expressed genes were the same with the two approaches

A

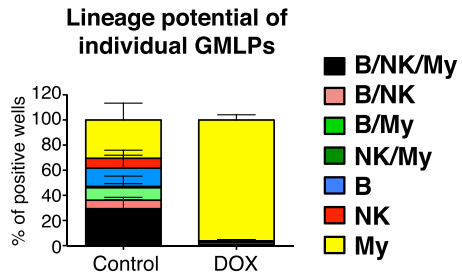

B

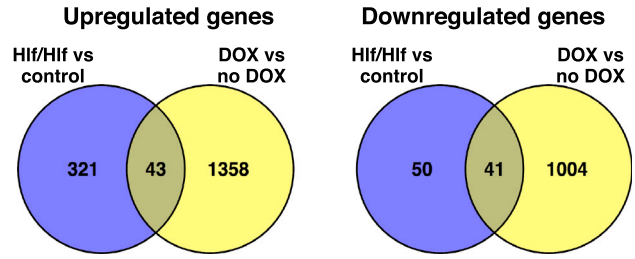

C

Commonly upregulated genes

	Fold change viral overexpression	Fold change transgenic mouse	Locus bound by Hlf?
Ces1d	605,8	112,6	
Gas6	97,0	15,1	
Eps8	94,9	6,9	yes
Adamtsl5	39,4	8,2	
Col5a2	32,8	24,9	
Sdc2	19,7	9,4	
Emr1	16,9	2,9	yes
Hlf	16,5	27,0	
Lpl	9,3	2,4	yes
Sytl4	8,6	3,3	
Pls3	8,0	2,9	
Maged1	7,8	2,5	
Nav1	7,7	2,5	yes
Aplp2	6,8	2,2	
Slc5a3	6,3	3,5	
Ptgds	4,7	3,1	
Syne2	4,5	4,8	
Pcdhga9	4,3	3,1	
Flnb	4,2	3,5	yes
Il15	4,1	4,4	yes
Pam	3,8	2,6	yes
Als2	3,6	2,6	yes
Sdc1	3,2	5,6	yes
Gcnt2	3,1	3,4	yes
Trps1	3,1	2,1	
Ndufa4	3,1	1,9	
Kit	3,0	7,7	
Pja2	3,0	2,0	
Tnfaip1	2,9	2,1	
Nfic	2,9	2,0	yes
Angptl2	2,8	3,3	
Ctnnd1	2,8	3,1	
Slc35d1	2,7	2,7	
Tspan6	2,7	3,1	
Stom	2,6	2,2	yes
Hip1	2,6	2,4	yes
Rbms2	2,6	1,8	
Vav3	2,4	1,8	yes
Atp8b4	2,3	2,8	yes
Ctnna1	2,1	2,2	yes
Nedd4	2,1	2,5	yes
Hk3	2,0	1,7	
Flna	1,9	2,6	yes

Commonly downregulated genes

	Fold change viral overexpression	Fold change transgenic mouse	Locus bound by Hlf?
Igha	-311,8	-1201,9	
Sh2d2a	-76,9	-7,2	
Prss30	-50,6	-151,1	
P2ry10	-46,2	-6,3	
Igj	-27,0	-257,3	
Cd6	-20,1	-11,5	yes
Tcrg-C1	-18,5	-23,8	yes
Lax1	-14,9	-3,9	
Tmem108	-9,4	-12,5	
Ly6d	-8,1	-85,8	
Lck	-7,5	-4,6	
Dntt	-7,1	-4,0	
Socs2	-6,9	-6,6	
Tox	-6,7	-7,1	
Sla2	-6,2	-8,0	
Il1r2	-5,9	-9,9	
Myl10	-5,1	-4,4	
Ctsw	-5,1	-7,3	
Gfra1	-4,8	-33,0	
Ifitm1	-4,5	-1,9	
Prss57	-4,2	-2,8	
Lat	-4,2	-1,5	
Arpp21	-4,1	-3,4	
Smim5	-3,6	-4,4	
St6gal1	-3,3	-5,4	yes
Fgr	-3,3	-3,1	
H2-Ob	-3,1	-1,8	
Pim2	-3,0	-2,4	
Cd7	-2,9	-43,1	
Dtnbp1	-2,8	-2,1	
Mn1	-2,8	-2,4	
Crip1	-2,7	-2,6	
Mgst2	-2,7	-2,2	yes
BC064078	-2,6	-3,9	
Rasal1	-2,4	-2,2	
Ociad2	-2,4	-2,1	
Spint2	-2,3	-2,0	
Lsp1	-2,1	-4,9	
AI467606	-2,1	-1,7	
Nkg7	-1,9	-2,2	
Ctr9	-1,9	-1,6	

D

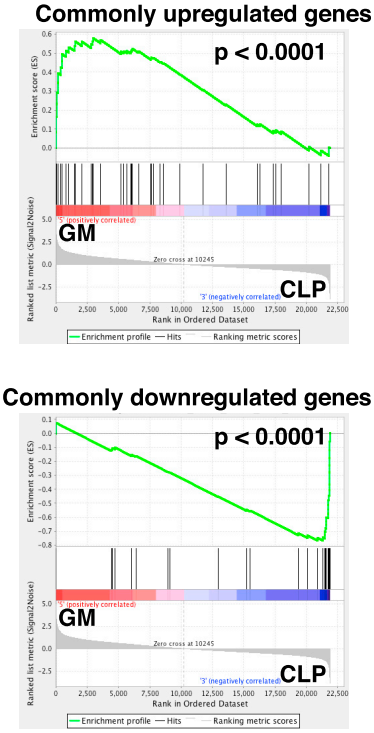

Figure 6. Hlf Instructs GMLPs to Adopt a Myeloid Fate by Upregulation of a Myeloid-Associated Transcriptional Program and a Concomitant Downregulation of Lymphoid-Affiliated Genes

(A) Single Hlf-inducible GMLPs were maintained on OP9 stromal cells for 14 days. The lineage potential of each seeded GMLP was determined using FACS, by scoring each well for the presence of B cells, NK cells, and myeloid cells. Shown is the distribution of the different colony types among the positive wells of the control and DOX treated groups.

(B) Venn diagrams depicting the number of shared up- and downregulated genes following Hlf induction using the two complementary approaches (compared with controls).

(C) Up- and downregulated genes, their fold changes compared with controls using both experimental strategies, and whether they were identified also using ChIP-seq. See also Table S2.

(D) GSEA in which the commonly up- and downregulated genes were used as gene sets and correlated against the whole transcriptomes of pGMs and CLPs. Error bars denote SEM. GSEA, gene set enrichment analysis. See also Figure S7.

(Figure 6C; Table S2). In addition, we found evidence for Hlf binding to 18 of the 43 upregulated genes, whereas only 4 of 41 downregulated genes presented as candidate Hlf targets (Figure 6C), perhaps suggesting that Hlf acts primarily to activate gene expression.

Next, we asked whether the up- and downregulated genes are part of larger transcriptional programs involved in early lympho- and myelopoiesis. Here, we used the up- and downregulated genes as gene sets for gene set enrichment analysis (GSEA) (Subramanian et al., 2005) and correlated the whole transcriptome of myeloid progenitors and CLPs against these genes (Figure 6D). Despite the very short induction period, this revealed striking associations of the upregulated genes with myeloid progenitors and downregulated genes to CLPs (Figure 6D),

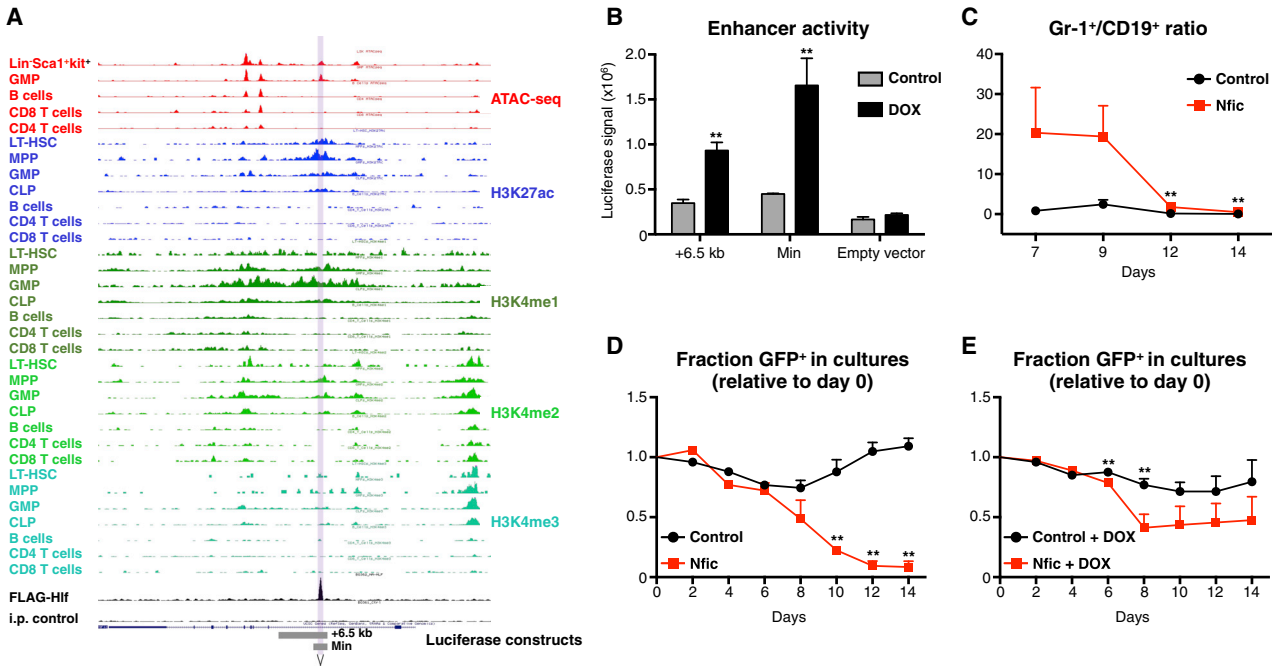

Figure 7. Identification of Nfic as a Direct Hlf Target with Pronounced Functional Effects on Hematopoietic Differentiation

(A) UCSC Genome Browser track depicting the genomic context of Nfic with regard to accessible chromatin and histone modifications of indicated cell types (assay for transposase-accessible chromatin using sequencing [ATAC-seq] and histone modification data from Lara-Astiaso et al. (2014). The region occupied by Hlf is highlighted.

(B) Luciferase reporter assay of the candidate Nfic enhancer using Hlf-inducible ESCs. Bars denote the mean firefly luciferase signal (±SEM) after normalization against *Renilla* using the +6.5 kb, a minimal (Min) enhancer construct, or an empty reporter construct, with or without Hlf induction (triplicate cultures from one of three representative experiments).

(C and D) Frequency of myeloid and B cells generated as a consequence of enforced Nfic expression. Shown are the ratios of percentage GFP$^+$ Gr1$^+$ myeloid cells over GFP$^+$CD19$^+$ B cells for the indicated groups. Data are from one of three experiments with similar results (n = 6 cultures per group for all cultures except day 14 Nfic, for which five cultures were analyzed). Enforced Nfic expression leads to a general loss of hematopoietic cells over time. Hlf-inducible GMLPs were maintained in the absence (C) or presence (D) of DOX and were transduced with either a control (Migr1) or Nfic retroviral vector and were subsequently cultured on OP9 stroma cells with monitoring every 2 days for frequency of GFP$^+$ cells (n = 1 replicate for days 0, 2, and 4 and n = 5 replicates for days 6, 8, 10, 12, and 14 for the groups in both C and D).

Error bars denote SEM. See also Figure S7.

emphasizing Hlf downregulation as a critical requirement for early lymphoid development.

Identification of the TF Nfic as a Direct Target Gene of Hlf

As a last part of our work, we explored whether we could identify any direct candidate target gene(s) of Hlf that might further detail its mechanism of action. For this, we generated retroviruses for 15 gene candidates selected on the basis of effect on transcription and chromatin binding (Figure 6C). Transduced cells were next assayed using the OP9 co-culture system. In preliminary analyses, the TF Nfic presented with both relative reductions in B cell and increases in myeloid output (Figure S7C). Closer interrogation of the chromatin environment around the Nfic-associated Hlf peak revealed a putative enhancer accessible in non-lymphoid cells (Figure 7A), and reporter assays in Hlf-inducible embryonic stem cells (ESCs) confirmed Hlf-dependent activation using both a larger domain covering the Hlf peak (+6.5 kb) and from a smaller domain (Min) restricted to encode the candidate Hlf-binding motifs (Figure 7B). However, although enforced Nfic expression had a strong and rapid negative effect on B cell output (Figure 7C), transgenic Nfic expression eventually also led to a reduction in myeloid cell output over time (Figure 7D), a feature not observed upon enforced Hlf expression alone (Figure 6A). Interestingly, when enforcing Hlf expression in the setting of Nfic overexpression, Hlf was able to counteract at least some of this reduction in cell output (Figure 7E), suggesting that the induction of Nfic alone cannot explain all the phenotypes observed upon persistent Hlf expression.

DISCUSSION

According to the prevailing view of hematopoiesis, appropriate blood cell formation is maintained in a hierarchical fashion and involves a range of progenitors with alternative differentiation and proliferation potentials. HSCs reside at the top of this hierarchy and have for decades been acknowledged as the primary cell type necessary for lifelong production of mature blood cells. Therefore, much focus has historically been aimed at isolation of near pure populations of HSCs. With this has come the

realization that the HSC pool might not be as homogeneous as initially assumed. Rather, the pool of HSCs might be composed of clones with alternative blood-forming potentials in terms of both lineage potential and the magnitude of the mature cells they give rise to (Goodell et al., 2015). Such "lineage-biased" HSC clones have been sub-classified by the retrospective functional readout of single-cell transplanted mice and/or by differential marker expression prior to functional assessment. However, caveats of such work include the difficulty in distinguishing HSCs with declining differentiation and/or self-renewal potential from HSCs that are truly biased toward a given lineage. It is therefore conceivable that assessments of mechanisms governing multipotency are more easily approached by the study of cells that reside more proximal to the decision points to be studied, including the GMLPs, which was the main cell type studied here.

Our gene expression profiling revealed Hlf to be highly expressed in multipotent GMLPs. A failure to downregulate Hlf at this developmental stage instructed GMLPs to adopt a myeloid fate and was incompatible with B, T, and NK cell development. When artificially turning Hlf into a transcriptional repressor by its fusion to the polycomb member M33, we observed a reciprocal phenotype, despite the otherwise highly lymphoid-permissive conditions that associates with the OP9 and OP9-DL1 differentiation systems. The failure to downregulate Hlf in GMLPs coincided with repression of lymphoid-affiliated genes and the concomitant induction of myeloid-associated genes, with many of the latter identified as candidate Hlf targets also by ChIP-seq.

An unexpected but to us highly interesting finding, given the involvement of Hlf in E2A-HLF driven acute B cell leukemia, was the prominent accumulation of a c-kit^{+}CD19^{+} population in the BM of Hlf-induced mice. Our approaches to characterize these cells collectively suggested that they represent committed B cell progenitors that are blocked in differentiation at a fraction B-C stage, which was further supported by a rapid gain of c-Kit expression of these cells upon Hlf induction. These cells also accumulated in the BM of WT mice transplanted with Hlf-inducible GMLPs, which coincided with a vastly decreased B cell reconstitution in the periphery. Given the genomic context of the E2A-HLF fusion oncogene, one outcome due to the more extended expression pattern of E2A should be aberrant expression of HLF in cell types normally devoid of HLF. However, as we have failed to observe leukemia upon Hlf induction, even following extensive time periods, additional mechanisms other than aberrant activation of Hlf target genes seem crucial for E2A-HLF-mediated transformation. At the same time, our studies appear in line with the observed phenotypes of murine transgenic models of the E2A-HLF fusion that manifest with myelo- rather than lymphoproliferation (Duque-Afonso et al., 2015).

By searching for candidate target genes of Hlf that could help explain the actions of Hlf on lineage commitment, we identified prominent Hlf binding to an intronic enhancer of Nfic and robust increases in Nfic mRNA expression upon Hlf induction. Although little is known about the role of Nfic in hematopoiesis, the Nfi family member Nfix was recently identified as a critical modulator of hematopoietic lineage choice by repressing B lymphoid formation while maintaining myeloid activity (O'Connor et al., 2015), suggesting redundancy among Nfi family members with respect to this activity. On the other hand, Nfic does not appear to explain all effects of Hlf, underscored not the least by a general loss of cells upon enforced Nfic expression. Although outside the scope of the current work, perhaps gene dosage and/or expression of alternative isoforms might underlie the differences observed between Nfic induced by Hlf and the retroviral approach we used, which does not exclude the likelihood that other target genes collaborate with Nfic to mediate a combined effect. When interrogating our Hlf ChIP-seq data (see Experimental Procedures, Data and Software Availability), we find Hlf binding to a recently identified distal c-Kit enhancer (chr5: 75,729,914–75,732,243) (Aranda-Orgilles et al., 2016). This might be relevant for our work, given the upregulation of c-Kit we see in the B cell lineage, the anti-apoptotic effect of c-kit signaling, and its downregulation in both B and T cell development (Godfrey et al., 1992; Rico-Vargas et al., 1994). Another potential candidate is the TF Meis1, whose promoter is occupied by Hlf (chr11: 18,741,886–19,157,511). In previous work from Kumar and colleagues (Roychoudhury et al., 2015), Meis1 was suggested to regulate Hlf expression, with Meis1 loss leading to pronounced apoptosis. Our observations extend these findings to include Hlf regulation of Meis1, indicative of a feedback loop between these factors.

As it is becoming increasingly apparent that multipotent progenitor cells other than HSCs are critical for steady-state hematopoiesis even over extended time periods (Busch et al., 2015; Sun et al., 2014), we believe that the ability of Hlf to strongly direct differentiation of an otherwise multipotent progenitor toward specific lineages is most relevant. A deeper understanding of the regulatory circuits governed by Hlf will not only be important to understand physiological blood cell formation but will likely also lead to an increased understanding of the leukemic processes that are characterized by involvement of Hlf.

EXPERIMENTAL PROCEDURES

Further details and an outline of resources used in this work can be found in Supplemental Experimental Procedures.

Generation of Viral Vectors

Viral constructs were generated using PCR-mediated Gibson Assembly and T4 DNA ligase cloning (New England Biolabs). Lentiviruses were produced by transient transfection of 293T producer cells and retroviruses by transient transfection into Plat-erythroid packaging cells.

Generation of Transgenic Mice and *In Vivo* Hlf Transgenic Strategy

DOX-inducible Hlf transgenic mice were generated by cloning the coding sequence and the 5′ and 3′ UTR of the murine Hlf gene into the pBS31 targeting vector (Beard et al., 2006). Next, the pBS31-Hlf construct was used to target KH2 ESCs by Flpase-mediated recombination (Beard et al., 2006). See Figure S3B for a schematic of the model. Following successful targeting, engineered ESCs were used to generate transgenic mice, which were backcrossed to CD45.1^{+} C57BL/6 mice and bred to homozygosity for the modified loci. Transgenic Hlf expression *in vivo* was achieved by administering DOX-containing chow *ad libitum* (2 g/kg; Bio-Serv). All animal experiments were performed with consent from a local ethics committee.

Immunophenotypic Analysis and Cell Sorting

For isolation and analysis of HSCs, the indicated progenitor populations and mature cells by FACS were performed as previously described (Inlay et al., 2009; Pronk and Bryder, 2011; Pronk et al., 2007; Tung et al., 2004).

In Vitro Evaluation of NK, B, and T Cell Potential by OP9/OP9-DL1 Co-culture

To determine the differentiation potential of Hlf-inducible GMLPs, cells were sorted directly into 48-well plates (bulk cultures) or 96-well plates (single-cell cultures) pre-plated with OP9 or OP9-DL1 stromal cells. In some experiments, WT GMLPs were instead first transduced viral vectors before stromal cell co-culture. B/NK cell permissive cultures were maintained on OP9 stroma cells in medium containing 20 ng/mL interleukin-15 (IL-15), 40 ng/mL IL-2, 10 ng/mL stem cell factor (SCF), 10 ng/mL fms-like tyrosine kinase 3 ligand (Flt3L), and 10 ng/mL IL-7, while T cells were generated on OP9-DL1 stroma supplemented with 10 ng/mL Flt3L and 10 ng/mL IL-7. Hlf-inducible cultures were maintained in the presence or absence of 1 μg/mL DOX (Sigma-Aldrich). Cultures were evaluated at the indicated time points by cell counting and FACS analysis.

Evaluation of Apoptosis

To investigate whether Hlf expression resulted in increased levels of apoptosis in B and T lymphoid progenitors, thymic $CD4^+CD8^+$ and BM-derived fraction B-C cells were FACS-sorted from Hlf-inducible mice and cultured on OP9-DL1 and OP9, respectively, with or without DOX (1 μg/mL) for 48 hr. Next, fraction B-C cultures were stained with a c-Kit antibody (2B8; eBioscience), and both culture types were thereafter incubated with annexin V conjugated to Cy5 and propidium iodide for 15 min before immediate FACS analysis.

Reconstitution Experiments

Eight thousand five hundred to 15,000 Hlf-inducible GMLPs ($CD45.1^+$) were transplanted into sublethally irradiated (500 rad) WT $CD45.2^+$ C57BL/6 recipient mice preconditioned for 5 days prior to transplantation by allowing mice to eat DOX-containing food. The mice were kept on a DOX pellet diet for 21 days (when investigating the effects of prolonged Hlf expression) or 22 days and 14 days followed by 8 days with a normal diet (when investigating the effect of DOX withdrawal on the established phenotypes) post-transplantation; BM, spleen, thymus, and PB of the recipient mice were analyzed for donor reconstitution.

Affymetrix Gene Expression Analysis and qRT-PCR

Microarray data were analyzed using dChip (Li and Hung Wong, 2001). For qRT-PCR experiments, the indicated populations were FACS-sorted directly into RLT lysis buffer and purified using the RNeasy Micro mRNA purification kit (QIAGEN), followed by first-strand cDNA synthesis as previously described (Norddahl et al., 2011). In some cases, the cDNA was amplified using KAPA HiFi Hotstart Readymix (Kapa Biosystems). qRT-PCRs were run with SYBR GreenER (Invitrogen) or EvaGreen (Bio-Rad).

ChIP-Seq Experiments

WT LSK cells were infected with a pMX-GFP control or a pMX-3xFLAG-Hlf/Hlf-IRES-GFP virus and grown for 5 days in basal OP9 medium supplemented with 50 ng/mL SCF, 10 ng/mL IL-7, 10 ng/mL Flt3L, and 5 ng/mL IL-3 (all from Peprotech). Next, 2×10^7 cells were cross-linked in 1% formaldehyde, and nuclei were prepared and snap-frozen in a dry ice/isopropanol bath. The frozen nuclei were lysed, and chromatin was sonicated in a Bioruptor (Diagenode) before immunoprecipitating with a FLAG-tag antibody (F3165; Sigma-Aldrich). Next, cross-links were reversed, and DNA was purified using QIAGEN PCR clean-up columns. Sequencing libraries were prepared using the Illumina TruSeq ChIP sample preparation kit (IP-202-1012; Illumina) and sequenced on an Illumina HiSeq 2500. Further details along with data-processing regimens can be found in Supplemental Experimental Procedures.

RNA-Seq

WT GMLPs were transduced with pHAGE2-Hlf/Hlf-IRES-ZsGreen or a pHAGE2 control virus, and Hlf-inducible GMLPs maintained in the presence or absence of DOX were cultured on OP9 stroma in B/NK cell conditions for 4 days. Next, $ZsGreen^+/CD45^+$ cells were FACS-sorted. Following RNA purification, libraries were prepared by the SMARTer Ultra Low Input RNA Kit for Sequencing (Clontech), and RNA-seq analysis was performed using an Illumina HiSeq 2500 platform by the Genome Technology Access Center (GTAC; Washington University School of Medicine). Data-processing details can be found in Supplemental Experimental Procedures.

B Cell Transdifferentiation Experiments

B cell-to-macrophage transdifferentiation experiments were performed in essence as previously described (Xie et al., 2004). In brief, 100,000 BM-resident $B220^+CD19^+$ B cells were isolated by FACS and transduced on retronectin-coated plates with a MigR1 control virus, MigR1-Hlf, and a MigR1-Cebpb virus and cultured on OP9 stroma for 4 days in basal OP9 medium supplemented with SCF, M-CSF, IL-3, IL-7, and Flt3L (all at 10 ng/mL) prior to FACS analysis.

VDJ Rearrangement PCR

The PCR reactions were run using 10,000 cells of each indicated population exactly as previously described (Schlissel et al., 1991).

Luciferase Assays

A 1 kb fragment containing the Hlf-bound region of the Nfic gene or a more specific 204 bp region containing three candidate HLF-binding sites was inserted into the pGL2 vector upstream of a SV40 promoter sequence and firefly luciferase reporter. The resulting vectors, or an empty pGL2 vector, were used to co-transfect Hlf-inducible ESCs maintained with or without DOX using Lipofectamine LTX reagent (Invitrogen) together with a *Renilla* luciferase reporter gene plasmid. Luciferase reporter signals were determined 24 hr post-transfection using the Dual-Luciferase Reporter Assay System kit (Promega).

Statistics

Data analysis was performed using Microsoft Excel and GraphPad Prism (GraphPad Software). All FACS data were analyzed with FlowJo (Tree Star). The heatmap in Figure 1B was prepared using GEN-E (http://www.broadinstitute.org/cancer/software/GENE-E/index.html). Venn diagrams were generated using Venny (Oliveros, 2007–2015). Significance values, with the exception of Figure 4A (splenic T cell reconstitution), for which a Mann-Whitney test was used, were calculated using Student's two-tailed t test, and a p value of <0.05 was considered to indicate statistical significance.

DATA AND SOFTWARE AVAILABILITY

The accession numbers for the microarray data reported in this paper are GEO: GSE44923 and GEO: GSE27686 (HSCs); GEO: GSE8407 (Pre Meg/erythroid, Pre CFU-erythroid, CFU-erythroid, MkP, pGM and CLP); GEO: GSE18734 (GMLP); and GEO: GSE14833 (GMP). The accession number for the generated ChIP-seq data reported in this paper is GEO: GSE69817. Our ChIP data can also be visualized using a custom University of California, Santa Cruz (UCSC), Genome Browser session (http://genome-euro.ucsc.edu/cgi-bin/hgTracks?hgS_doOtherUser=submit&hgS_otherUserName=promufa&hgS_otherUserSessionName=Lund_160719) together with previously established ChIP data (Lara-Astiaso et al., 2014). The accession number for the RNA-seq data reported in this paper is GEO: GSE69858.

SUPPLEMENTAL INFORMATION

Supplemental Information includes Supplemental Experimental Procedures, seven figures, and two tables and can be found with this article online at https://doi.org/10.1016/j.celrep.2017.10.112.

AUTHOR CONTRIBUTIONS

M.W. and D.B. designed the study. M.W., V.L., I.H., P.S., H.W., M.D.-P. and G.L.N. performed experiments. M.M. provided intellectual input. V.L.,

M.S.C., R.H., and B.G. were involved in the design, interpretation, and analysis of the ChIP-seq experiment. D.B. conceived and supervised the study and wrote the paper together with M.W.

ACKNOWLEDGMENTS

This work was generously supported by project grants to D.B. from the Swedish Cancer Society, the Swedish Medical Research Council, the Swedish Pediatric Leukemia Foundation, the Knut and Alice Wallenberg Foundation, and an European Research Council (ERC) consolidator grant (615068). Work in the Gottgens lab is supported by the Wellcome Trust, CRUK, Bloodwise, MRC, NIH-NIDDK, and core support funding by the Wellcome Trust and MRC to the Cambridge Stem Cell Institute. We would like to acknowledge Tom Serwold, Ewa Sitnicka, and Mikael Sigvardsson for valuable scientific discussions and Eva Erlandsson and Gerd Sten for expert technical assistance. The GTAC, Department of Genetics, Washington University School of Medicine, assisted with genomic analysis and is partially supported by National Cancer Institute (NCI) Cancer Center Support Grant P30 CA91842 to the Siteman Cancer Center, Institute of Clinical and Translational Sciences (ICTS)/Clinical and Translational Science Award (CTSA) Grant UL1TR000448 from the National Center for Research Resources (NCRR; a component of the NIH), and the NIH Roadmap for Medical Research.

Received: June 28, 2017
Revised: September 11, 2017
Accepted: October 28, 2017
Published: November 21, 2017

REFERENCES

Adolfsson, J., Månsson, R., Buza-Vidas, N., Hultquist, A., Liuba, K., Jensen, C.T., Bryder, D., Yang, L., Borge, O.J., Thoren, L.A., et al. (2005). Identification of Flt3+ lympho-myeloid stem cells lacking erythro-megakaryocytic potential a revised road map for adult blood lineage commitment. Cell *121*, 295–306.

Akashi, K., Traver, D., Miyamoto, T., and Weissman, I.L. (2000). A clonogenic common myeloid progenitor that gives rise to all myeloid lineages. Nature *404*, 193–197.

Allman, D., Sambandam, A., Kim, S., Miller, J.P., Pagan, A., Well, D., Meraz, A., and Bhandoola, A. (2003). Thymopoiesis independent of common lymphoid progenitors. Nat. Immunol. *4*, 168–174.

Aranda-Orgilles, B., Saldaña-Meyer, R., Wang, E., Trompouki, E., Fassl, A., Lau, S., Mullenders, J., Rocha, P.P., Raviram, R., Guillamot, M., et al. (2016). MED12 regulates HSC-specific enhancers independently of mediator kinase activity to control hematopoiesis. Cell Stem Cell *19*, 784–799.

Argiropoulos, B., Yung, E., Xiang, P., Lo, C.Y., Kuchenbauer, F., Palmqvist, L., Reindl, C., Heuser, M., Sekulovic, S., Rosten, P., et al. (2010). Linkage of the potent leukemogenic activity of Meis1 to cell-cycle entry and transcriptional regulation of cyclin D3. Blood *115*, 4071–4082.

Arinobu, Y., Mizuno, S., Chong, Y., Shigematsu, H., Iino, T., Iwasaki, H., Graf, T., Mayfield, R., Chan, S., Kastner, P., and Akashi, K. (2007). Reciprocal activation of GATA-1 and PU.1 marks initial specification of hematopoietic stem cells into myeloerythroid and myelolymphoid lineages. Cell Stem Cell *1*, 416–427.

Beard, C., Hochedlinger, K., Plath, K., Wutz, A., and Jaenisch, R. (2006). Efficient method to generate single-copy transgenic mice by site-specific integration in embryonic stem cells. Genesis *44*, 23–28.

Benz, C., Martins, V.C., Radtke, F., and Bleul, C.C. (2008). The stream of precursors that colonizes the thymus proceeds selectively through the early T lineage precursor stage of T cell development. J. Exp. Med. *205*, 1187–1199.

Bryder, D., Rossi, D.J., and Weissman, I.L. (2006). Hematopoietic stem cells: the paradigmatic tissue-specific stem cell. Am. J. Pathol. *169*, 338–346.

Busch, K., Klapproth, K., Barile, M., Flossdorf, M., Holland-Letz, T., Schlenner, S.M., Reth, M., Höfer, T., and Rodewald, H.R. (2015). Fundamental properties of unperturbed haematopoiesis from stem cells in vivo. Nature *518*, 542–546.

Duque-Afonso, J., Smith, K.S., and Cleary, M.L. (2015). Conditional expression of E2A-HLF induces B-cell precursor death and myeloproliferative-like disease in knock-in mice. PLoS ONE *10*, e0143216.

Fischer, U., Forster, M., Rinaldi, A., Risch, T., Sungalee, S., Warnatz, H.J., Bornhauser, B., Gombert, M., Kratsch, C., Stütz, A.M., et al. (2015). Genomics and drug profiling of fatal TCF3-HLF-positive acute lymphoblastic leukemia identifies recurrent mutation patterns and therapeutic options. Nat. Genet. *47*, 1020–1029.

Forsberg, E.C., Serwold, T., Kogan, S., Weissman, I.L., and Passegué, E. (2006). New evidence supporting megakaryocyte-erythrocyte potential of flk2/flt3+ multipotent hematopoietic progenitors. Cell *126*, 415–426.

Gachon, F., Fonjallaz, P., Damiola, F., Gos, P., Kodama, T., Zakany, J., Duboule, D., Petit, B., Tafti, M., and Schibler, U. (2004). The loss of circadian PAR bZip transcription factors results in epilepsy. Genes Dev. *18*, 1397–1412.

Gachon, F., Olela, F.F., Schaad, O., Descombes, P., and Schibler, U. (2006). The circadian PAR-domain basic leucine zipper transcription factors DBP, TEF, and HLF modulate basal and inducible xenobiotic detoxification. Cell Metab. *4*, 25–36.

Gazit, R., Garrison, B.S., Rao, T.N., Shay, T., Costello, J., Ericson, J., Kim, F., Collins, J.J., Regev, A., Wagers, A.J., and Rossi, D.J.; Immunological Genome Project Consortium (2013). Transcriptome analysis identifies regulators of hematopoietic stem and progenitor cells. Stem Cell Reports *1*, 266–280.

Germain, R.N. (2002). T-cell development and the CD4-CD8 lineage decision. Nat. Rev. Immunol. *2*, 309–322.

Godfrey, D.I., Zlotnik, A., and Suda, T. (1992). Phenotypic and functional characterization of c-kit expression during intrathymic T cell development. J. Immunol. *149*, 2281–2285.

Goodell, M.A., Nguyen, H., and Shroyer, N. (2015). Somatic stem cell heterogeneity: diversity in the blood, skin and intestinal stem cell compartments. Nat. Rev. Mol. Cell Biol. *16*, 299–309.

Hardy, R.R., and Hayakawa, K. (2001). B cell development pathways. Annu. Rev. Immunol. *19*, 595–621.

Hardy, R.R., Carmack, C.E., Shinton, S.A., Kemp, J.D., and Hayakawa, K. (1991). Resolution and characterization of pro-B and pre-pro-B cell stages in normal mouse bone marrow. J. Exp. Med. *173*, 1213–1225.

Hunger, S.P., Ohyashiki, K., Toyama, K., and Cleary, M.L. (1992). Hlf, a novel hepatic bZIP protein, shows altered DNA-binding properties following fusion to E2A in t(17;19) acute lymphoblastic leukemia. Genes Dev. *6*, 1608–1620.

Inaba, T., Roberts, W.M., Shapiro, L.H., Jolly, K.W., Raimondi, S.C., Smith, S.D., and Look, A.T. (1992). Fusion of the leucine zipper gene HLF to the E2A gene in human acute B-lineage leukemia. Science *257*, 531–534.

Inaba, T., Shapiro, L.H., Funabiki, T., Sinclair, A.E., Jones, B.G., Ashmun, R.A., and Look, A.T. (1994). DNA-binding specificity and trans-activating potential of the leukemia-associated E2A-hepatic leukemia factor fusion protein. Mol. Cell. Biol. *14*, 3403–3413.

Inlay, M.A., Bhattacharya, D., Sahoo, D., Serwold, T., Seita, J., Karsunky, H., Plevritis, S.K., Dill, D.L., and Weissman, I.L. (2009). Ly6d marks the earliest stage of B-cell specification and identifies the branchpoint between B-cell and T-cell development. Genes Dev. *23*, 2376–2381.

Inukai, T., Inaba, T., Dang, J., Kuribara, R., Ozawa, K., Miyajima, A., Wu, W., Look, A.T., Arinobu, Y., Iwasaki, H., et al. (2005). TEF, an antiapoptotic bZIP transcription factor related to the oncogenic E2A-HLF chimera, inhibits cell growth by down-regulating expression of the common beta chain of cytokine receptors. Blood *105*, 4437–4444.

Ji, H., Ehrlich, L.I., Seita, J., Murakami, P., Doi, A., Lindau, P., Lee, H., Aryee, M.J., Irizarry, R.A., Kim, K., et al. (2010). Comprehensive methylome map of lineage commitment from haematopoietic progenitors. Nature *467*, 338–342.

Kamizono, S., Duncan, G.S., Seidel, M.G., Morimoto, A., Hamada, K., Grosveld, G., Akashi, K., Lind, E.F., Haight, J.P., Ohashi, P.S., et al. (2009). Nfil3/E4bp4 is required for the development and maturation of NK cells in vivo. J. Exp. Med. *206*, 2977–2986.

Kondo, M., Weissman, I.L., and Akashi, K. (1997). Identification of clonogenic common lymphoid progenitors in mouse bone marrow. Cell *91*, 661–672.

Lara-Astiaso, D., Weiner, A., Lorenzo-Vivas, E., Zaretsky, I., Jaitin, D.A., David, E., Keren-Shaul, H., Mildner, A., Winter, D., Jung, S., et al. (2014). Immunogenetics. Chromatin state dynamics during blood formation. Science *345*, 943–949.

Li, C., and Hung Wong, W. (2001). Model-based analysis of oligonucleotide arrays: model validation, design issues and standard error application. Genome Biol. *2*, RESEARCH0032.

Mercer, E.M., Lin, Y.C., and Murre, C. (2011). Factors and networks that underpin early hematopoiesis. Semin. Immunol. *23*, 317–325.

Mitsui, S., Yamaguchi, S., Matsuo, T., Ishida, Y., and Okamura, H. (2001). Antagonistic role of E4BP4 and PAR proteins in the circadian oscillatory mechanism. Genes Dev. *15*, 995–1006.

Nakano, T., Kodama, H., and Honjo, T. (1994). Generation of lymphohematopoietic cells from embryonic stem cells in culture. Science *265*, 1098–1101.

Norddahl, G.L., Pronk, C.J., Wahlestedt, M., Sten, G., Nygren, J.M., Ugale, A., Sigvardsson, M., and Bryder, D. (2011). Accumulating mitochondrial DNA mutations drive premature hematopoietic aging phenotypes distinct from physiological stem cell aging. Cell Stem Cell *8*, 499–510.

O'Connor, C., Campos, J., Osinski, J.M., Gronostajski, R.M., Michie, A.M., and Keeshan, K. (2015). Nfix expression critically modulates early B lymphopoiesis and myelopoiesis. PLoS ONE *10*, e0120102.

Oliveros, J.C. (2007–2015). Venny 2.1. http://bioinfogp.cnb.csic.es/tools/venny/index.html.

Pronk, C.J., and Bryder, D. (2011). Flow cytometry-based identification of immature myeloerythroid development. Methods Mol. Biol. *699*, 275–293.

Pronk, C.J., Rossi, D.J., Månsson, R., Attema, J.L., Norddahl, G.L., Chan, C.K., Sigvardsson, M., Weissman, I.L., and Bryder, D. (2007). Elucidation of the phenotypic, functional, and molecular topography of a myeloerythroid progenitor cell hierarchy. Cell Stem Cell *1*, 428–442.

Pronk, C.J., Attema, J., Rossi, D.J., Sigvardsson, M., and Bryder, D. (2008). Deciphering developmental stages of adult myelopoiesis. Cell Cycle *7*, 706–713.

Rico-Vargas, S.A., Weiskopf, B., Nishikawa, S., and Osmond, D.G. (1994). c-kit expression by B cell precursors in mouse bone marrow. Stimulation of B cell genesis by in vivo treatment with anti-c-kit antibody. J. Immunol. *152*, 2845–2852.

Riddell, J., Gazit, R., Garrison, B.S., Guo, G., Saadatpour, A., Mandal, P.K., Ebina, W., Volchkov, P., Yuan, G.C., Orkin, S.H., and Rossi, D.J. (2014). Reprogramming committed murine blood cells to induced hematopoietic stem cells with defined factors. Cell *157*, 549–564.

Roychoudhury, J., Clark, J.P., Gracia-Maldonado, G., Unnisa, Z., Wunderlich, M., Link, K.A., Dasgupta, N., Aronow, B., Huang, G., Mulloy, J.C., and Kumar, A.R. (2015). MEIS1 regulates an HLF-oxidative stress axis in MLL-fusion gene leukemia. Blood *125*, 2544–2552.

Sanjuan-Pla, A., Macaulay, I.C., Jensen, C.T., Woll, P.S., Luis, T.C., Mead, A., Moore, S., Carella, C., Matsuoka, S., Bouriez Jones, T., et al. (2013). Platelet-biased stem cells reside at the apex of the haematopoietic stem-cell hierarchy. Nature *502*, 232–236.

Schlissel, M.S., Corcoran, L.M., and Baltimore, D. (1991). Virus-transformed pre-B cells show ordered activation but not inactivation of immunoglobulin gene rearrangement and transcription. J. Exp. Med. *173*, 711–720.

Schmitt, T.M., and Zúñiga-Pflücker, J.C. (2002). Induction of T cell development from hematopoietic progenitor cells by delta-like-1 in vitro. Immunity *17*, 749–756.

Shojaei, F., Trowbridge, J., Gallacher, L., Yuefei, L., Goodale, D., Karanu, F., Levac, K., and Bhatia, M. (2005). Hierarchical and ontogenic positions serve to define the molecular basis of human hematopoietic stem cell behavior. Dev. Cell *8*, 651–663.

Subramanian, A., Tamayo, P., Mootha, V.K., Mukherjee, S., Ebert, B.L., Gillette, M.A., Paulovich, A., Pomeroy, S.L., Golub, T.R., Lander, E.S., and Mesirov, J.P. (2005). Gene set enrichment analysis: a knowledge-based approach for interpreting genome-wide expression profiles. Proc. Natl. Acad. Sci. U S A *102*, 15545–15550.

Sun, J., Ramos, A., Chapman, B., Johnnidis, J.B., Le, L., Ho, Y.J., Klein, A., Hofmann, O., and Camargo, F.D. (2014). Clonal dynamics of native haematopoiesis. Nature *514*, 322–327.

Tung, J.W., Parks, D.R., Moore, W.A., Herzenberg, L.A., and Herzenberg, L.A. (2004). Identification of B-cell subsets: an exposition of 11-color (Hi-D) FACS methods. Methods Mol. Biol. *271*, 37–58.

Wahlestedt, M., Norddahl, G.L., Sten, G., Ugale, A., Frisk, M.A., Mattsson, R., Deierborg, T., Sigvardsson, M., and Bryder, D. (2013). An epigenetic component of hematopoietic stem cell aging amenable to reprogramming into a young state. Blood *121*, 4257–4264.

Weishaupt, H., Sigvardsson, M., and Attema, J.L. (2010). Epigenetic chromatin states uniquely define the developmental plasticity of murine hematopoietic stem cells. Blood *115*, 247–256.

Xie, H., Ye, M., Feng, R., and Graf, T. (2004). Stepwise reprogramming of B cells into macrophages. Cell *117*, 663–676.

Yamamoto, R., Morita, Y., Ooehara, J., Hamanaka, S., Onodera, M., Rudolph, K.L., Ema, H., and Nakauchi, H. (2013). Clonal analysis unveils self-renewing lineage-restricted progenitors generated directly from hematopoietic stem cells. Cell *154*, 1112–1126.

Yang, Q., Jeremiah Bell, J., and Bhandoola, A. (2010). T-cell lineage determination. Immunol. Rev. *238*, 12–22.

Zuber, A.M., Centeno, G., Pradervand, S., Nikolaeva, S., Maquelin, L., Cardinaux, L., Bonny, O., and Firsov, D. (2009). Molecular clock is involved in predictive circadian adjustment of renal function. Proc. Natl. Acad. Sci. U S A *106*, 16523–16528.

Cell Reports, Volume *21*

Supplemental Information

Critical Modulation of Hematopoietic Lineage Fate by Hepatic Leukemia Factor

Martin Wahlestedt, Vasileios Ladopoulos, Isabel Hidalgo, Manuel Sanchez Castillo, Rebecca Hannah, Petter Säwén, Haixia Wan, Monika Dudenhöffer-Pfeifer, Mattias Magnusson, Gudmundur L. Norddahl, Berthold Göttgens, and David Bryder

SUPPLEMENTARY INFORMATION

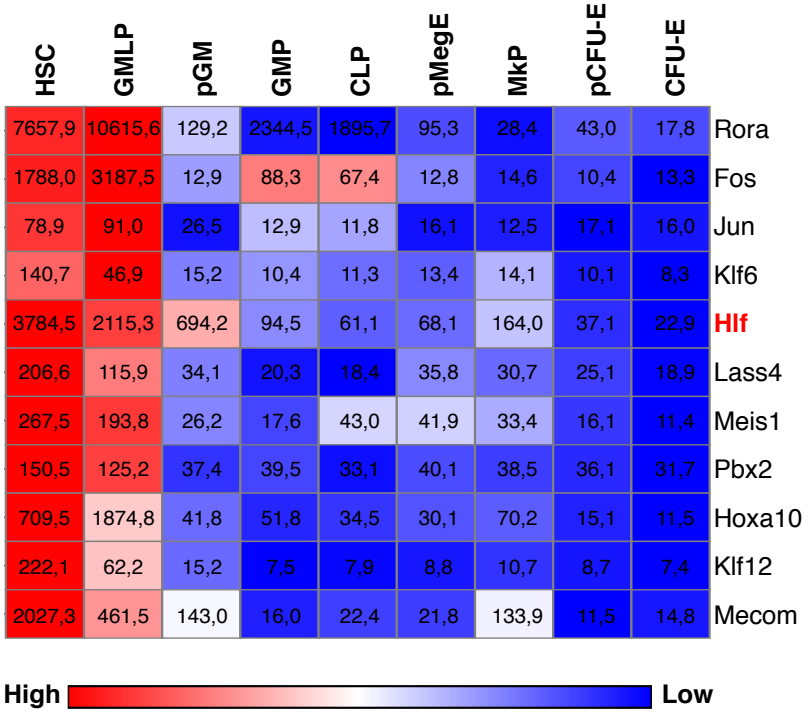

Figure S1

Figure S1. Extended heatmap of transcription factors with 2-fold or higher expression levels in HSCs and GMLPs compared to downstream progenitor subsets (related to Figure 1). The heatmap shown in Figure 1B is depicted along with the probe level expression values.

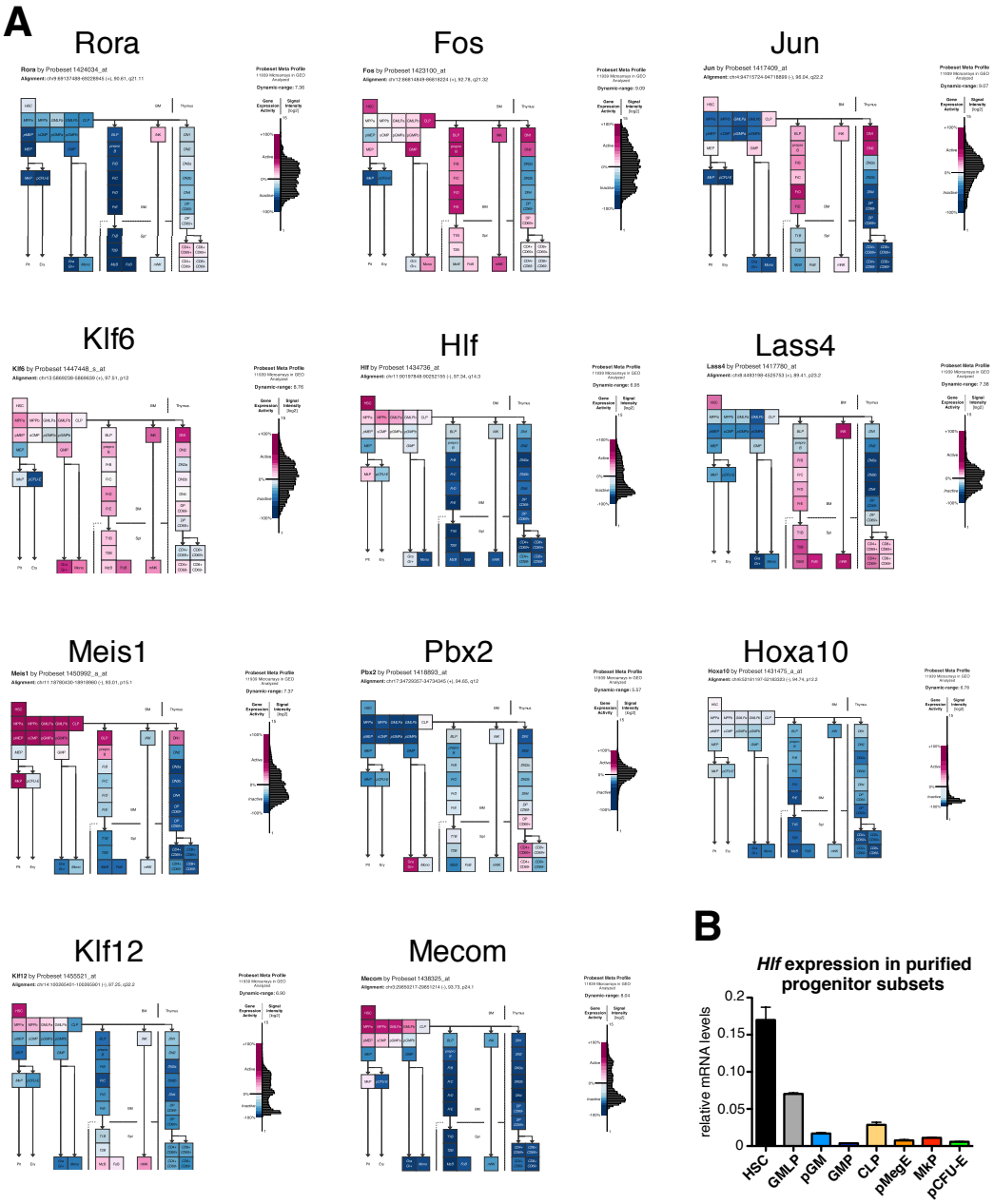

Figure S2. Expression profiles from Gene Expression Commons of the 11 identified HSC and GMLP specific transcription factors and qRT-PCR validation of Hlf expression levels in primary hematopoietic progenitors (related to Figure 1). (A) Hematopoietic gene expression profiles from Gene Expression commons (https://gexc.riken.jp) of identified transcription factors. (B) Hlf mRNA expression levels in the indicated stem and progenitor subsets as determined by qRT-PCR and expressed relative to Actb (3 replicates/cell type from one of two experiments with similar results). qRT-PCR; quantitative Real Time-Polymerase Chain Reaction.

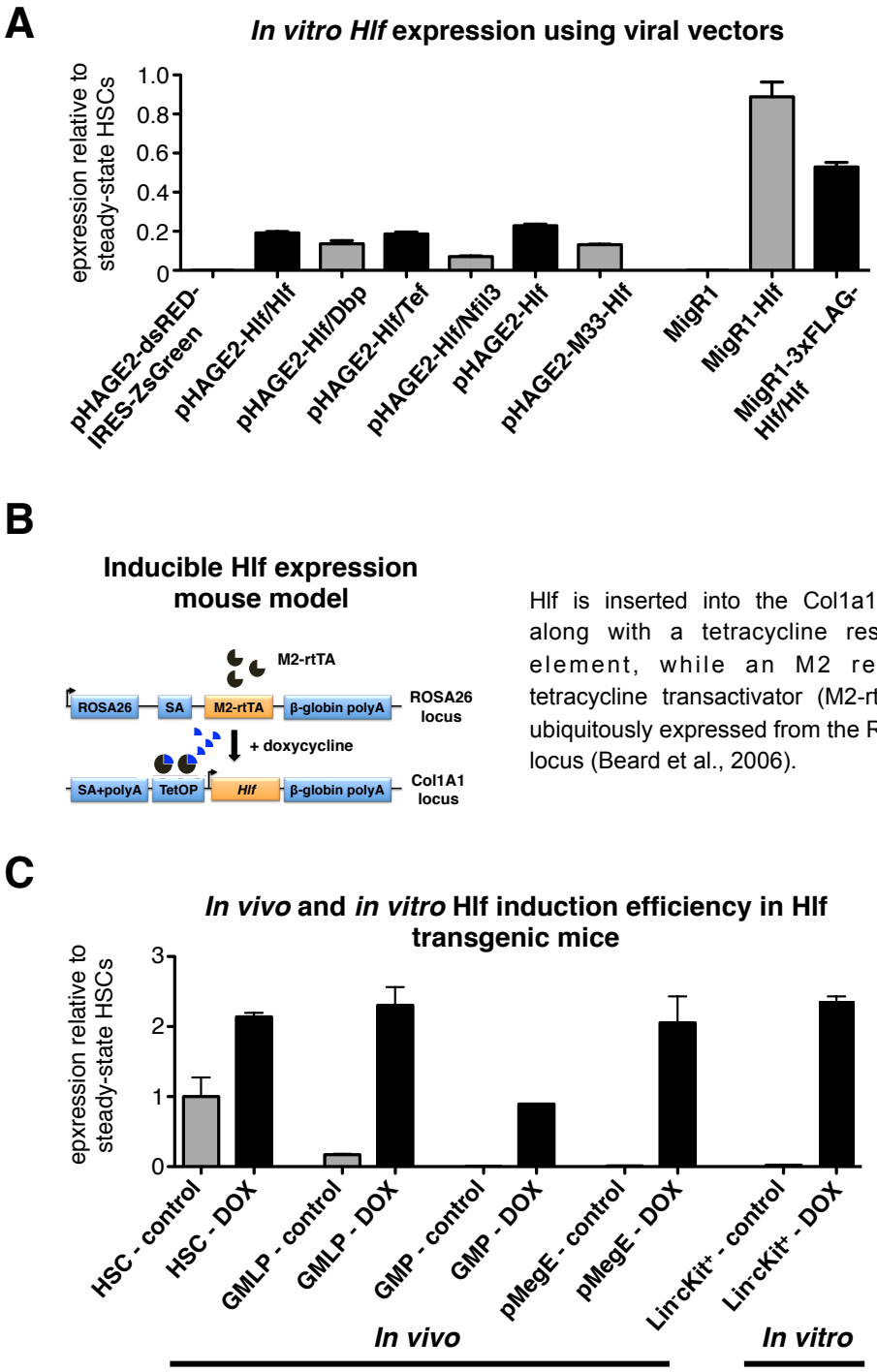

Figure S3. Validation of the Hlf-based viral constructs (*in vitro*) and schematic depicition and validation of the inducible Hlf mouse model (related to Figure 1). (A) Hlf expression levels in FACS sorted GFP+ transduced cells using the viral vectors in the work (3 replicates for each vector). (B) Schematic depiction of the Hlf conditional transgenic mouse model. A reverse tetracycline transactivator (M2-rtTA) is driven from the Rosa26 locus, which, upon the addition of DOX can bind to the TetOP and drive the expression of the single-copy Hlf transgene inserted into the Col1a1 locus. (C) Hlf expression levels in depicted cell subsets using the inducible Hlf transgenic mouse (3 replicates for each cell type and treatment). Error bars depict SEM. TetOP; Tetracycline Operon, SA; Splice Acceptor.

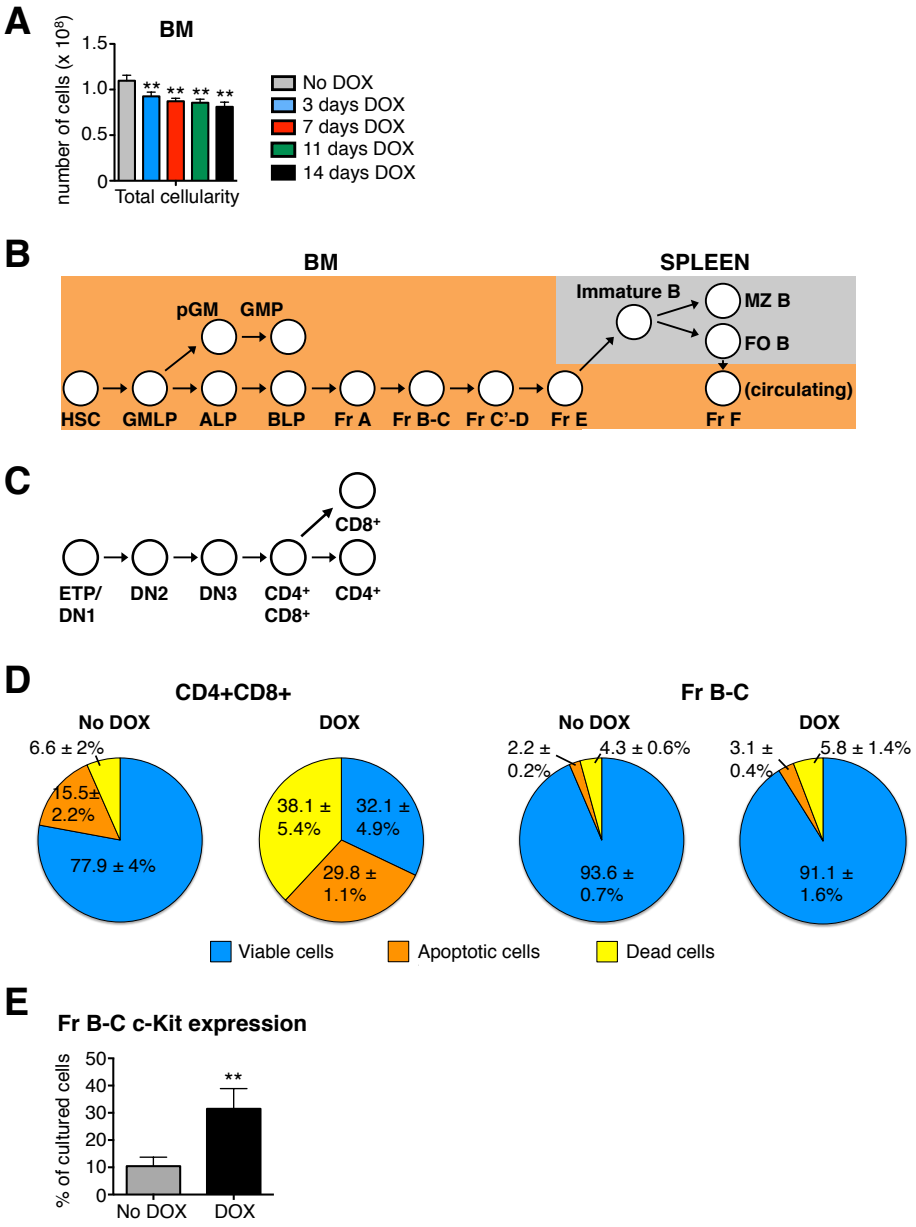

Figure S4. Hematopoietic effects of in vivo Hlf induction and specific investigation into the Hlf-associated loss of immature lymphocytes (related to Figure 2). (A) Bar charts showing the overall BM cellularity in Hlf induced mice. (B) Overview of the various analyzed cell fractions and their proposed developmental relationships. (C) Overview of the various analyzed cell fractions in the thymus and their proposed developmental relationships. (D) $CD4^+CD8^+$ thymocytes and Fraction B-C B-lymphocytes were cultured for 48h in the absence or presence of DOX on OP9-DL1 and OP9 stromal cell respectively before staining with Annexin V and Propidium Iodide. Pie charts show the degree of cell viability (average ± SEM), apoptosis and death for both cell types (n = 6 replicates per group, from one of two experiments with similar results). (E) Fraction B-C B-lymphocytes treated as in (D) were investigated for c-Kit expression using FACS (n = 6, one experiment). Bar graph shows the average percentage of $c\text{-}Kit^+$ cells in Fraction B-C cultures. Error bars denote SEM.

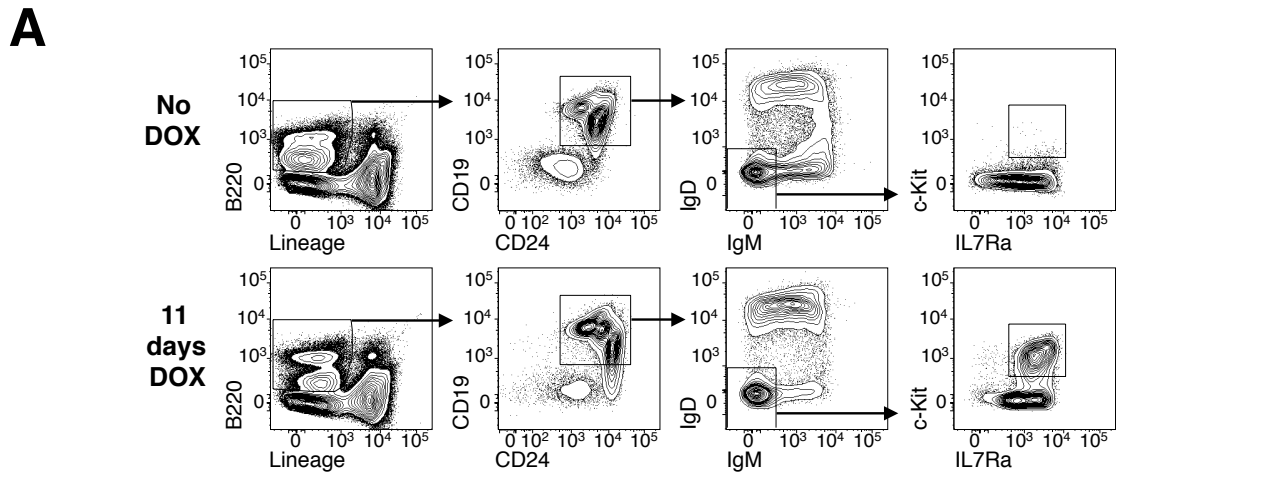
A
No DOX
11 days DOX
B220
Lineage
CD19
CD24
IgD
IgM
c-Kit
IL7Ra

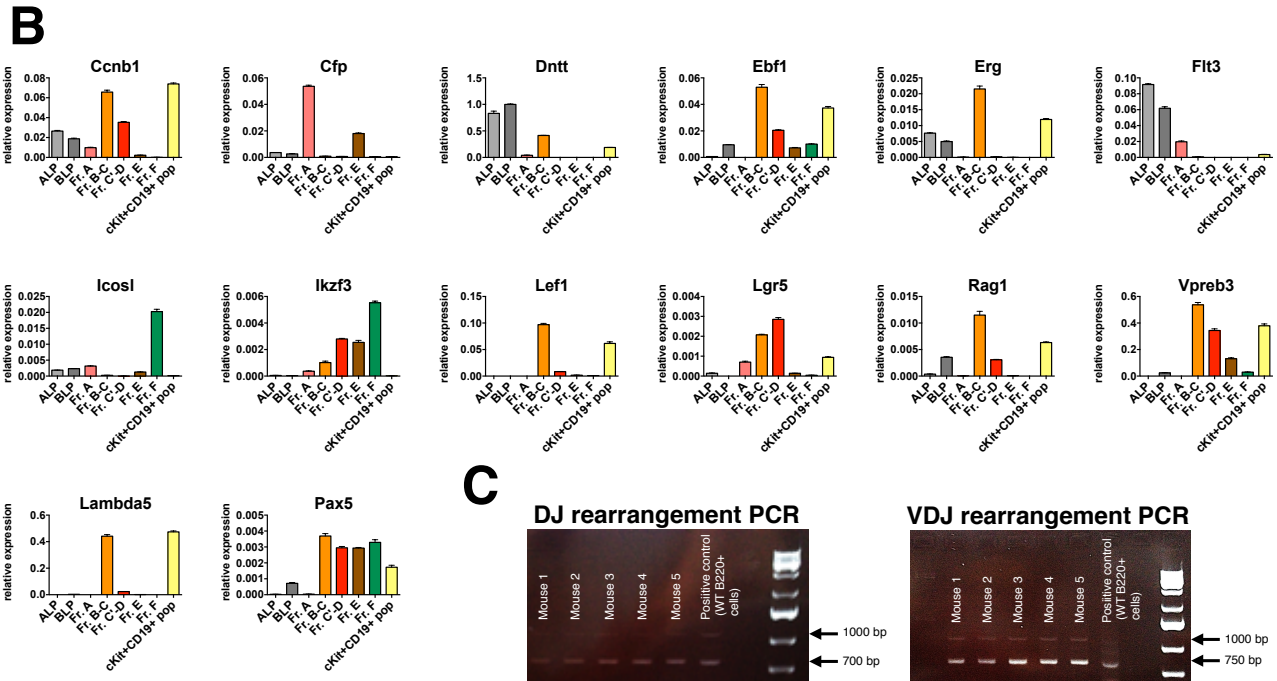
B
Ccnb1
Cfp
Dntt
Ebf1
Erg
Flt3
Icosl
Ikzf3
Lef1
Lgr5
Rag1
Vpreb3
Lambda5
Pax5
relative expression
ALP BLP Fr. A Fr. B-C Fr. C'-D Fr. E Fr. F cKit+CD19+ pop

C
DJ rearrangement PCR
VDJ rearrangement PCR
Mouse 1
Mouse 2
Mouse 3
Mouse 4
Mouse 5
Positive control (WT B220+ cells)
1000 bp
700 bp
333 bp
750 bp
350 bp

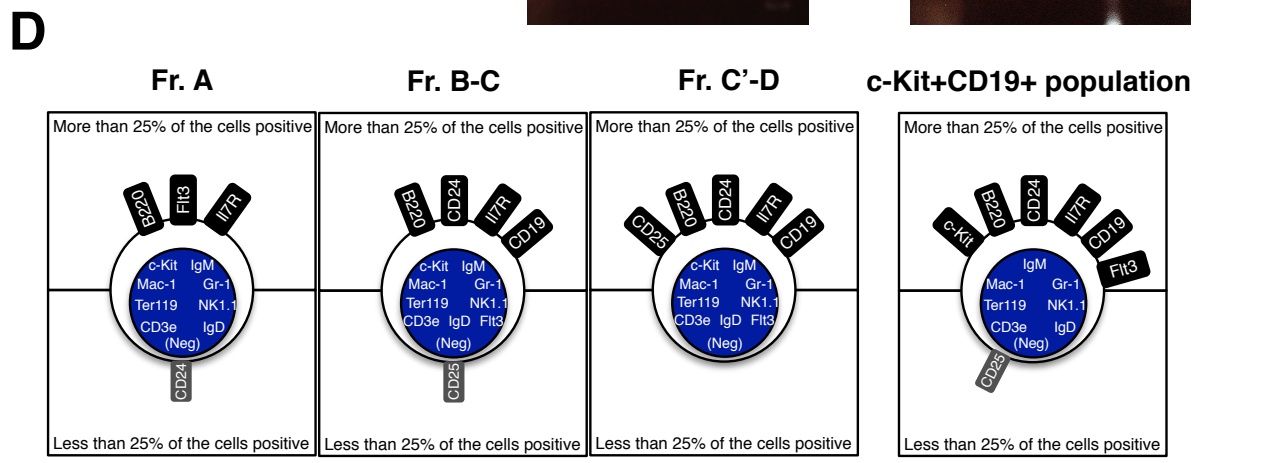
D
Fr. A
Fr. B-C
Fr. C'-D
c-Kit+CD19+ population
More than 25% of the cells positive
Less than 25% of the cells positive
B220
Flt3
Il7R
CD24
CD19
CD25
c-Kit
IgM
Mac-1
Gr-1
Ter119
NK1.1
CD3e
IgD
(Neg)

Figure S5 (related to Figure 2). Characterization of Hlf induced Lin$^-$ B220$^+$CD19$^+$CD24$^+$IgM$^-$IgD$^-$c-Kit$^+$IL7Ra$^+$ cells. (A) Representative FACS plots showing the appearance of B220$^+$CD19$^+$CD24^{+l}L7Ra$^+$c-Kit$^+$ cells in the BM following enforced Hlf expression. (B) The expression levels of Ccnb1, Cfp, Dntt, Ebf1, Erg, Flt3, Icosl, Ikzf3, Lambda5, Lef1, Lgr5, Pax5, Rag1 and Vpreb3 were determined in Lin$^-$ B220$^+$CD19$^+$CD24$^+$IgM$^-$IgD$^-$c-Kit$^+$IL7Ra$^+$ cells and compared to those in ALPs, BLPs, Fr. A, Fr. B-C, Fr. C'-D, Fr. E and Fr. F cells (n = 3 replicates per cell type and gene, from one experiment). (C) (TOP) Heavy chain DJ rearrangement and (BOTTOM) heavy chain VDJ rearrangement measured by PCR in Lin$^-$B220$^+$CD19$^+$CD24$^+$IgM$^-$IgD$^-$c-Kit$^+$IL7Ra$^+$ cells (from 5 individual mice) and compared to BM resident B220+ cells in WT mice. Arrows depict the expected bands. (D) Schematic diagrams showing the cell surface marker phenotype of Lin$^-$B220$^+$CD19$^+$CD24$^+$IgM$^-$IgD$^-$c-Kit$^+$IL7Ra$^+$ cells compared to Fr. A, Fr. B-C and Fr. C'-D. Error bars denote SEM.

A

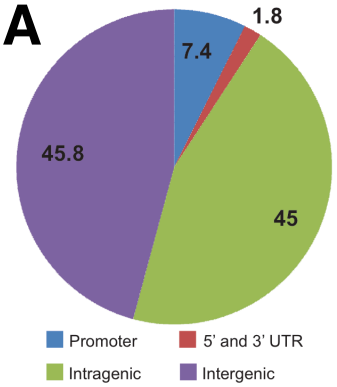

B

Summary

Name	MA0043.1
Alt. Name	HLF
Database	JASPAR non redun _vertebrate_MEME.txt
***p*-value**	2.00984e-05
***E*-value**	0.00261279
***q*-value**	0.00254512
Overlap	10
Offset	1
Orientation	Normal

Alignment

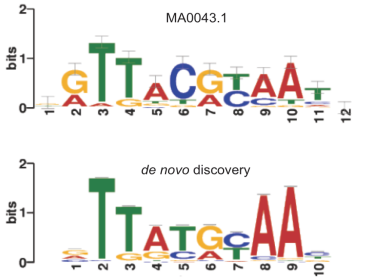

C

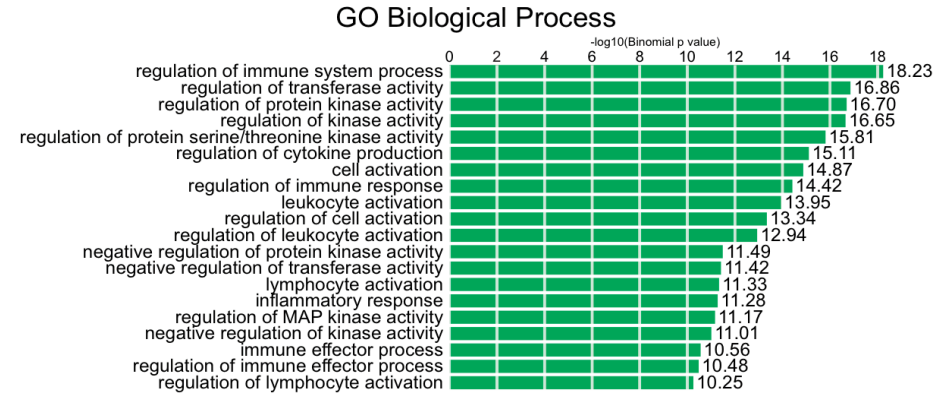

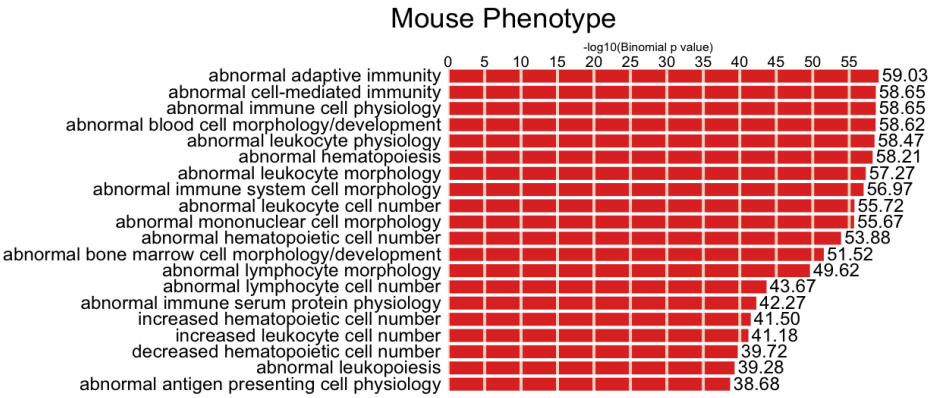

D

Rank	Motif	P-value	log P-pvalue	% of Targets	% of Background	STD(Bg STD)	Best Match/Details
1		1e-1960	-4.515e+03	57.37%	2.57%	30.8bp (63.4bp)	MF0006.1_bZIP_cEBP-like_subclass/Jaspar More Information | Similar Motifs Found
2		1e-369	-8.511e+02	26.13%	4.53%	51.0bp (57.4bp)	PB0058.1_Sfpi1_1/Jaspar More Information | Similar Motifs Found
3		1e-130	-2.997e+02	22.87%	8.54%	52.9bp (61.1bp)	RUNX(Runt)/HPC7-Runx1-ChIP-Seq/Homer More Information | Similar Motifs Found
4		1e-122	-2.821e+02	3.39%	0.10%	26.0bp (59.4bp)	MA0138.2_REST/Jaspar More Information | Similar Motifs Found
5		1e-88	-2.030e+02	2.79%	0.11%	31.8bp (61.6bp)	MA0138.1_REST/Jaspar More Information | Similar Motifs Found
6		1e-54	-1.257e+02	10.31%	3.87%	55.4bp (60.1bp)	PU.1-IRF(ETS:IRF)/Bcell-PU.1-ChIP-Seq(GSE21512)/Homer More Information | Similar Motifs Found
7		1e-37	-8.688e+01	6.76%	2.44%	53.3bp (60.6bp)	Jun-AP1(bZIP)/K562-cJun-ChIP-Seq/Homer More Information | Similar Motifs Found
8		1e-23	-5.472e+01	2.76%	0.74%	60.6bp (57.5bp)	CTCF(Zf)/CD4+-CTCF-ChIP-Seq/Homer More Information | Similar Motifs Found

Figure S6 (related to Figure 5). Genome-wide Hlf binding characteristics. (A) Pie chart displaying the distribution of the identified Hlf peaks in different genomic regions (graph obtained using CEAS (Shin et al., 2009), available on cistrome.org/ap/). (B) Sequence logo showing the deduced Hlf binding motif (HOMER de novo discovery) and the binding motif for human HLF in the JASPAR database (MA0043.1). (C) Gene ontology categories and mouse phenotypes associated with the putative Hlf targets determined using GREAT analysis (http://www.great.stanford.edu) (McLean et al., 2010) ranked in a decreasing likelihood order. (D) Sequence logos showing the 8 most overrepresented TF motifs in the Hlf peaks as obtained from HOMER *de novo* motif discovery.

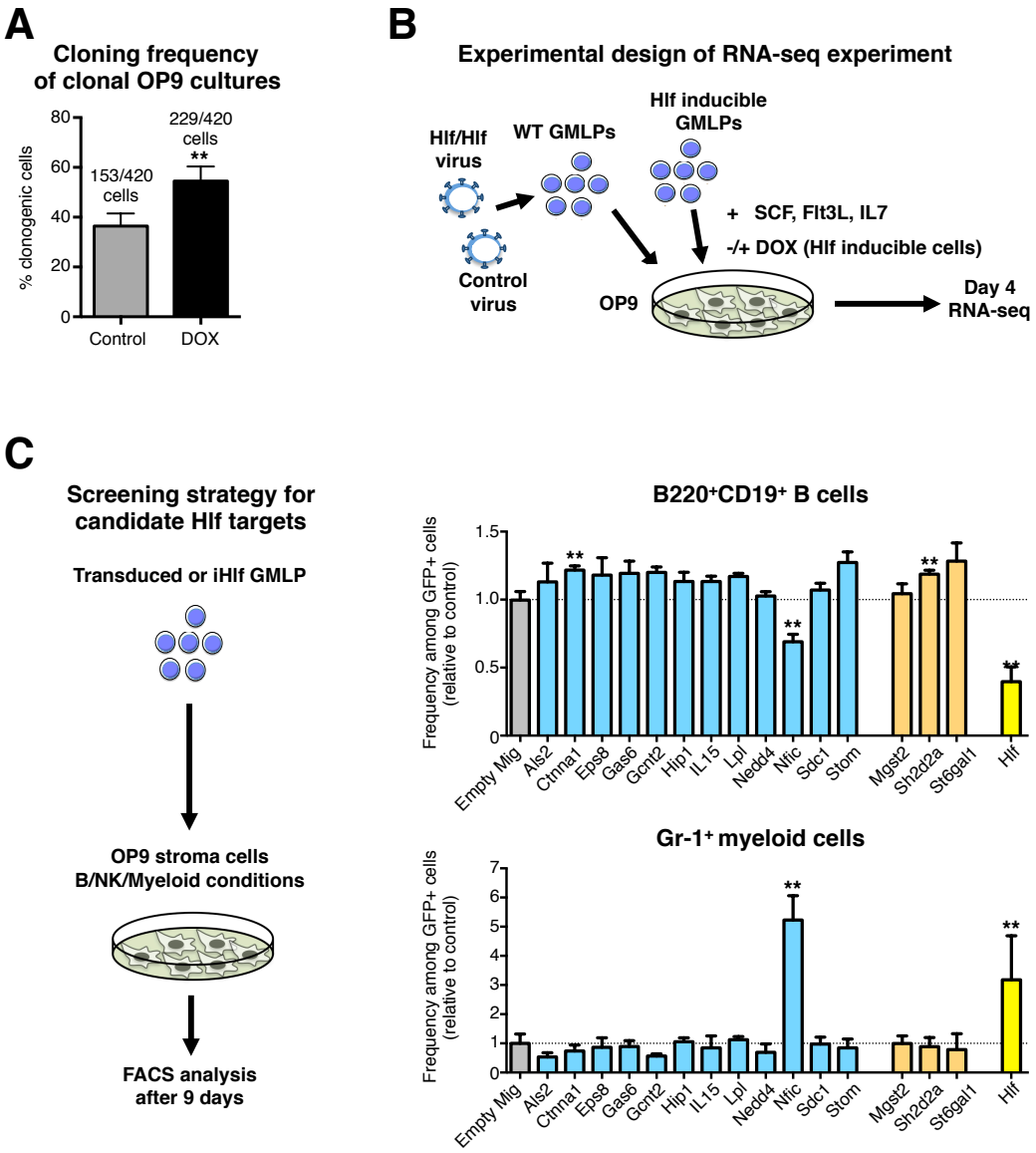

Figure S7 (related to Figure 6 and 7). Cloning frequency of Hlf-inducible GMLPs, the experimental outline for RNA-seq experiments and functional screening of candidate Hlf targets. (A) Cloning frequency (defined as percent of the total number of seeded wells containing at least 30 B-, NK or myeloid cells) of cultures initiated with GMLPs in the absence or presence of Hlf induction (420 initiated cultures/group from 5 independent experiments). (B) Schematic outline for the RNA sequencing experiments; WT GMLPs transduced with the Hlf/Hlf construct or a control virus (see Figure 1) and Hlf inducible GMLPs maintained in the absence or presence of DOX were cultured for 4 days on OP9 stroma under B cell permissive conditions, prior to processing for RNA sequencing (duplicate samples per group). (C) Bicistronic retroviral vectors for indicated genes and GFP were generated and used to transduce GMLPs. Cells were subsequently evaluated using the OP9 stromal co-culture system for their ability to produce myeloid and lymphoid cells following 9 days of culture (n = 3 replicates per vector, from one experiment). Error bars depict SEM.

SUPPLEMENTAL EXPERIMENTAL PROCEDURES

Construction of viral vectors and production of high-titer viruses

All viral constructs unless indicated were constructed using PCR-mediated Gibson Assembly cloning (New England Biolabs). In brief, the single-copy Hlf gene construct was generated by PCR amplification of the coding sequence of Hlf with the addition of a N-terminal HA-tag and assembly into a BamHI and NotI (New England Biolabs) linearized pHAGE2 vector (Mostoslavsky et al., 2005). The single-copy Nfil3 construct was generated by PCR amplification of the Nfil3 coding sequence with 5' addition of a NotI restriction enzyme site and 3' addition of a BamHI restriction enzyme site, A-tailing using Taq DNA polymerase (VWR), TA-cloning into the pCR2.1 plasmid (Invitrogen), restriction enzyme digestion of the Nfil3 fragment by BamHI and NotI (New England Biolabs) and ligation into a BamHI and NotI linearized pHAGE2 vector using T4 DNA ligase (New England Biolabs). For the Hlf based forced dimer constructs, the coding sequence of Hlf was amplified without a stop codon with an incorporated linker sequence (Neuhold and Wold, 1993) and assembled into pHAGE2 along with the coding sequences of Hlf, Tef, Dbp and Nfil3. To generate the vector used for the ChIP-seq experiments, the coding sequence of an Hlf/Hlf homodimer was first PCR amplified with the addition of an N-terminal 3xFLAG tag (GACTACAAAGACCATGACGGTGATTATAAAGATCATGATATCGATTACAAGGATGA CGATGACAAG) and assembled into BamHI and NotI linearized pHAGE2. Next, the 3xFLAG-Hlf/Hlf fragment along with an IRES element was PCR amplified and assembled into a NcoI linearized pMX-GFP retroviral vector (Cell Biolabs). The M33-Hlf lentiviral fusion construct was generated by fusing the repressive domain of M33 to the coding sequence of Hlf as described for Meis1 (Argiropoulos et al., 2010) with the addition of a N-terminal 3xFLAG tag, followed by cloning into a BamHI and NotI linearized pHAGE2 vector. The retroviral M33-Hlf fusion construct was generated by PCR amplification of 3xFLAG-M33-Hlf from the pHAGE2 vector and assembly into EcoRI and XhoI linearized MigR1 retroviral vector (Pear et al., 1998). The lentiviral M33-Hlf fusion construct was generated in an identical manner but assembled into the pHAGE2 vector. The constructs used for transdifferentiation experiments were generated by PCR amplification of single-copy Hlf and Cebpb and assembled into a EcoRI and XhoI linearized MigR1 (Pear et al., 1998). To generate the retroviral vectors containing the selected candidate Hlf targets, the coding sequences of each gene was PCR amplified and assembled into a EcoRI and XhoI linearized MigR1 (Pear et al., 1998). All Hlf based constructs were designed to retain a minimal Kozak sequence (ATCACG). The gene products for the Hlf, M33, Dbp, Nfil3 and Tef constructs were PCR amplified using the Q5 High-Fidelity DNA Polymerase (New England Biolabs) from a full-length cDNA library generated from unfractionated BM cells using the Qiagen RNeasy Micro Kit (Qiagen) and Superscript III (Invitrogen). The gene products for Als2, Ctnna1, Eps8, Gas6, Gcnt2, Hip1, Il15, Lpl, Mgst2, Nedd4, Nfic, Sdc1, Sh2d2a, St6gal1 and Stom were PCR amplified using the Q5 High-Fidelity DNA Polymerase (New England Biolabs) from full-length cDNA libraries generated from unfractionated BM cells, with the exception of Gas6 that was generated from testis cDNA, using the RNeasy Micro mRNA purification kit, with first- and second-strand synthesis carried out using Superscript II (Invitrogen). The resulting cDNA was next amplified using KAPA HiFi Hotstart Readymix (Kapa Biosystems Inc.). Lentiviruses were produced by transient transfection of 293T producer cells using Lipofectamine LTX (Invitrogen) with the lentiviral plasmids and

packaging constructs (HDM-Hgpm2, HDM-Tat1b, HDM-VSVG and RC-CMV-Rev1b). Lentiviral supernatants were harvested 48 and 72h post transfection and concentrated by ultracentrifugation. The retroviral supernatants were produced by Lipofectamine LTX transfection of Plat-E packaging cells (Cell Biolabs) with the retroviral vectors, followed by harvest of the supernatants 48h post transfection.

Generation of transgenic mice and in vivo Hlf transgenic strategy

To generate DOX inducible Hlf transgenic mice, the conserved coding sequence, along with the 5' and 3' UTR of the murine Hlf gene was subcloned from the pYX-Asc-Hlf plasmid (K.K. DNAFORM) into the pBS31 targeting vector (Beard et al., 2006). Next, the targeting construct was inserted in the Col1a1 locus via Flpase mediated recombination into the KH2 ES cell line (Beard et al., 2006). See also Figure S3B for a schematic depiction of the model. Specific integration of the targeting construct and the presence of the reverse tetracycline transactivator in the Rosa26 locus was verified by PCR. Following karyotyping and test of Hlf inducibility in vitro, engineered ES cells were injected into E3.5 C57Bl/6 blastocysts and implanted into pseudopregnant mice at the Transgenic Core Facility at Lund University. Following germline transmission, mice were backcrossed to CD45.1$^+$ C57BL/6 mice and bred to homozygozity for both the modified Col1a1 and Rosa26 loci. To achieve transgenic expression of Hlf in vivo, transgenic mice or mice transplanted with Hlf inducible GMLPs were administered DOX-containing chow (or normal food in control mice) ad libitum (2 g/kg, Ssniff Specialdiäten). All animal experiments were performed with consent from a local ethical committee.

Immunophenotypic analysis and cell sorting

For isolation and analysis of HSCs, the indicated progenitor populations and mature cells by FACS were performed as previously described (Inlay et al., 2009; Pronk and Bryder, 2011; Pronk et al., 2007; Tung et al., 2004). In brief, single-cell suspensions from BM, spleen, thymus and peripheral blood were prepared and stained with fluorescently labeled antibodies and subjected to FACS analysis and/or sorting. In some cases, overall organ cellularity was also assessed using a Sysmex KX-21 N machine (Sysmex) and intersected with FACS data to determine the absolute number of the indicated cell fractions in the different organs. For cell sorting, cell suspensions were depleted of mature hematopoietic cells using biotinylated antibodies against B220 (RA3-6B2), Gr-1 (RB6-8C5), CD11b (M1/70), CD8a (53–6.7), Ter-119, CD4 (GK1.5) (all from Biolegend) and anti-biotin MACS beads (Miltenyi Biotec), and was followed by staining with fluorescently labeled antibodies. Cell sorting was performed on FACS Aria I,II and III cell sorters and analysis on an LSRII (Becton Dickinson). The immunophenotypes of the cells used for FACS analysis and sorting were: HSC; Lin$^-$cKit$^+$Sca1$^+$CD48$^-$CD150$^+$, GMLP; Lin$^-$cKit$^+$Sca1$^+$CD48$^+$CD150$^-$Flt3$^+$, pGM; Lin$^-$cKit$^+$Sca1$^-$CD105$^-$CD150$^-$CD16/32$^-$, GMP; Lin$^-$cKit$^+$Sca1$^-$CD105$^-$CD150$^-$CD16/32$^+$, ALP; Lin$^-$cKit^{low}Sca1^{low}Flt3$^+$IL7Ra$^+$Ly6D$^-$, BLP; Lin$^-$Kit^{low}Sca1^{low}Flt3$^+$IL7Ra$^+$Ly6D$^+$, pMegE; Lin$^-$cKit$^+$Sca1$^-$CD105$^-$CD150$^+$CD41$^-$, pCFU-E; Lin$^-$cKit$^+$Sca1$^-$CD105$^+$CD150$^+$CD41$^-$, CFU-E; Lin$^-$cKit$^+$Sca1$^-$CD105$^+$CD150$^-$CD41$^-$, MkP; Lin$^-$cKit$^+$Sca1$^-$CD150$^+$CD41$^+$, Fr. A; Lin$^-$B220$^+$CD19$^-$CD24$^-$IgM$^-$IgD$^-$, Fr. B-C; Lin$^-$B220$^+$CD19^{high}CD24^{low}IgM$^-$IgD$^-$, Fr. C'-D; Lin$^-$B220$^+$CD19^{low}CD24^{high}IgM$^-$IgD$^-$, Fr. E;

$Lin^-B220^+CD19^{low}CD24^{high}IgM^+IgD^-$, Fr. F; $Lin^-B220^+CD19^{high}CD24^{low}IgM^{-/+}IgD^{-/+}$, Follicular B; $Lin^-B220^+CD19^+IgM^{low}IgD^+CD21^+$, Marginal Zone B; $Lin^-B220^+CD19^+IgM^+IgD^{low}CD5^-CD43^-CD21^+$, Immature B; $Lin^-B220^+CD19^+IgM^+IgD^{low}CD5^-CD43^-CD21^-$, ETP/DN1; $Lin^-CD4^-CD8^-cKit^+CD25^-$; DN2; $Lin^-CD4^-CD8^-cKit^+CD25^+$; DN3; $Lin^-CD4^-CD8^-cKit^-CD25^+$; CD4+CD8+; $Lin^-CD4^+CD8^+cKit^-CD25^-$; CD4+; $Lin^-CD4^+CD8^-cKit^-CD25^-$; CD8+; $Lin^-CD4^-CD8^+cKit^-CD25^-$.

In vitro evaluation of NK-, B-, and T cell potential by OP9/OP9-DL1 coculture

To determine the differentiation potential of bulk sorted GMLPs from Hlf inducible mice (Figure 1E), cells were sorted into 48-well plates pre-plated with OP9 (Kodama et al., 1994) or OP9-DL1 stromal cells. The lineage potential of single GMLPs was assessed by culturing individually FACS-deposited GMLPs in OP9 coated 96-well plates. For assessments of the differentiation potential following the lentiviral transduction in Figure 1D, 3,000 WT GMLPs were transduced twice during 36h on retronectin-coated plates (Takara) and were next divided over three wells of a 6-well plate pre-plated with OP9 or OP9-DL1 stromal cells. For the experiments involving the M33-Hlf fusion construct shown in Figure 4B and 4C, 2,000 WT GMLPs were transduced overnight with a retroviral M33-Hlf vector on retronectin-coated plates (Takara) and were subsequently divided over three wells of a 6-well plate pre-plated with OP9 and three wells pre-plated with OP9-DL1 stromal cells. To investigate effects of candidate Hlf targets, 2,600 WT GMLPs were transduced on retronectin-coated plates overnight with the indicated viruses and were thereafter divided over three wells of a 6-well plate pre-plated with OP9 and three wells pre-plated with OP9-DL1 stromal cells. To evaluate the effect of Nfic overexpression, 32,000 GMLPs were sorted and prestimulated in OptiMEM and cytokines for 6h. Cells were next retrovirally transduced on retronectin-coated 96-well plates (Takara). After 24h, cells were split (between 100 and 5,000 cells) onto OP9 cells preplated 3h before. Frequencies of GFP+ cells were analyzed every 48h by FACS for 14 days. For B/NK cell permissive cultures, cells were grown on OP9 stroma cells and supplemented with 20 ng/mL interleukin 15 (IL-15), 40 ng/mL IL-2, 10 ng/mL Stem Cell Factor (SCF), 10 ng/mL fms-like tyrosine kinase 3 ligand (Flt3L), and 10 ng/mL IL-7. For T cell generation, cells were grown on OP9-DL1 stroma supplemented with 10 ng/mL Flt3L, and 10 ng/mL IL-7. The cocultures were maintained in the presence or absence of 1 ug/ml DOX (Sigma-Aldrich) and evaluated at the indicated time points by cell counting and FACS staining with CD19 (1D3), B220 (RA3-6B2), Gr-1 (RB6-8C5), NK1.1 (PK136) and PI for B- and NK cell OP9 cocultures, and CD19 (1D3), CD90.2/Thy1.2 (53-2.1), CD25 (7D4), c-Kit (2B8) and PI for T cell OP9-DL1 cocultures. The basal medium for maintaining the OP9/OP9-DL1 stromal cells, as well as the cocultures, was OptiMEM (Invitrogen), 10% fetal calf serum (Sigma-Aldrich), 50 µg/mL gentamicin (Invitrogen) and 50µM β-mercaptoethanol (Invitrogen). The OP9 and OP9-DL1 stroma cells were pre-plated 3h prior to the addition of hematopoietic cells at a seeding density of 2,000 cells/cm^2.

Evaluation of apoptosis

To investigate whether Hlf expression resulted in increased levels of apoptosis in B and T lymphoid progenitors, 100,000 thymic $CD4^+CD8^+$ and 100,000 bone marrow-derived Fraction B-C cells ($Lin^-B220^+CD19^{high}CD24^{low}IgM^-IgD^-$) were FACS sorted from Hlf inducible mice and cultured at 37ºC in wells of a 24-well plate preplated with 10,000 OP9-DL1 and 10,000 OP9 respectively in the absence or presence of DOX (1 ug/ml) for 48h. Next, the cells were harvested and the Fraction B-C cultures were first stained with a c-Kit antibody (2B8, eBioscience) for 30 min. Thereafter, both culture types were incubated with Annexin V conjugated to Cy5 and Propidium Iodide for 15 minutes before immediate FACS analysis. The OP9 cultures were maintained in basal OP9/OP9-DL1 medium supplemented with 10 ng/ml Flt3L, 10 ng/ml IL-7 and 50 ng/ml SCF, while the OP9-DL1 cultures were maintained in basal medium supplemented with 10 ng/ml Flt3L, 10 ng/ml IL-2 and 10 ng/ml IL-7.

Affymetrix gene expression analysis and qRT-PCR

The microarray data in Figure 1B and S1 can be found in the Gene Expression Omnibus (GEO) (HSC accession numbers GSE44923 and GSE27686) (Pre Meg/E, Pre CFU-E, CFU-E, MkP, pGM and CLP, accession number GSE8407) (GMLP, accession number GSE18734) (GMP, accession number GSE14833). For data preprocessing, probe level expression values were extracted using RMAExpress (Bolstad et al., 2003) and analyses were performed using the dChip software (Li and Hung Wong, 2001) by filtering out probes with a lower expression than 50 in all subsets to eliminate noise in expression, followed by fold-change calculations and hierarchical clustering. For the quantitative RT-PCR (qRT-PCR) experiments described in Figure S1 and S2, the indicated cellular fractions were FACS sorted directly into RLT lysis buffer and purified using the RNeasy Micro mRNA purification kit (Qiagen), followed by first-strand cDNA synthesis as previously described (Norddahl et al., 2011). qRT-PCR reactions were run with SYBR GreenER (Invitrogen). For the qRT-PCR experiments depicted in Figure S5B, RNA from the sorted populations was purified using the RNeasy Micro mRNA purification kit, but was followed by first-strand and second-strand synthesis using Superscript II (Invitrogen) and amplification using KAPA HiFi Hotstart Readymix (Kapa Biosystems Inc.) and used for qRT-PCR using EvaGreen (Bio-rad).

ChIP-seq

80,000 WT $Lin^-Sca\text{-}1^+c\text{-}Kit^+$ cells were infected on retronectin coated plates (Takara) with either a pMX-GFP control or a pMX-3xFLAG-Hlf/Hlf-IRES-GFP virus and maintained for 5 days in basal OP9 medium supplemented with 50 ng/ml SCF, 10 ng/ml IL-7, 10 ng/ml Flt3L and 5 ng/ml IL-3 (all from Peprotech). Next, 2 x 10^7 cells were cross-linked in 1% formaldehyde for 12 min at room temperature with constant stirring before quenching the crosslinking reaction by the addition of glycine to a concentration of 0.125M and incubation for 5 min at room temperature. Cells were washed and nuclei were prepared by incubation on ice in lysis buffer (10 mM Tris pH8.0, 10 mM NaCl, 0.2% NP40 containing protease inhibitors (protease inhibitor cocktail (Sigma) and PMSF) for

10 min. The nuclei were harvested by centrifugation at 600 x g for 5 minutes at 4° C and snap-frozen in a dry ice/isopropanol bath. The frozen nuclei were resuspended in 1 ml of nuclei lysis buffer (50mM Tris pH 8.0, 10mM EDTA, 1% SDS) containing protease inhibitors (as above) and incubated on ice for 10 minutes. An equal volume of IP dilution buffer (20mM Tris pH 8.0, 2mM EDTA, 150mM NaCl, 1% Triton X-100, 0.01% SDS) containing protease inhibitors was added and chromatin was sonicated in a Bioruptor (Diagenode) for 4 cycles (30s on, 30s off). The chromatin solution was centrifuged for 10 minutes at 3220 x g and the supernatant was transferred to a new tube. An additional 3 ml of IP buffer was added together with 50 µl of rabbit IgG (2 µg/µl) and incubated at 4° C for 1 hour. 200µl of Protein G sepharose beads (1:1 slurry in IP dilution buffer) were added to the chromatin solution and further incubated at 4° C for 2 hours. The beads/IgG were collected by centrifugation at 1800 x g for 2 minutes. The chromatin was transferred to 1.5 ml tubes, an input sample was removed and 7 µg anti-FLAG (F3165, Sigma-Aldrich) were added then incubated overnight at 4° C with rotation. 60µl of protein G agarose beads (1:1 slurry in IP dilution buffer) were added and incubated with the samples for 2 hours. The beads were harvested at 5400 x g for 2 minutes and washed twice with low salt buffer (20mM Tris pH 8.0, 2mM EDTA, 50mM NaCl, 1% Triton X-100, 0.1% SDS), then once with LiCl buffer (10mM Tris pH 8.0, 1mM EDTA, 0.25M LiCl, 1% NP40, 1% Sodium deoxycholate monohydrate) and twice with 1x TE pH 8.0. The complexes were eluted twice from the beads by adding 150µl elution buffer (100mM NaHCO3, 1% SDS). To reverse the cross-linking and deproteinate the samples, 0.3M NaCl, RnaseA and Proteinase K were added to all the IP samples and input, followed by overnight incubation at 65° C. DNA was purified using Qiagen PCR clean up columns. Sequencing libraries were prepared using the Illumina TruSeq ChIP Library preparation kit (IP-202-1012, Illumina) according to the manufacturers instructions. Libraries were quantified using the KAPA universal library quantification kit (KK4824, KAPA Biosystems) and the average size estimated using an Agilent Bioanalyzer with an Agilent DNA 1000 chip (Agilent Technologies). Libraries were sequenced on a Illumina HiSeq 2500. Raw sequence reads in fastq format were mapped to the mouse genome (Genome Reference Consortium Mouse Build 38 - mm10) using Bowtie2 (Langmead and Salzberg, 2012). Peak regions were called using MACS2 (Zhang et al., 2008) and density plots generated in bigWig format. These were then displayed together as custom tracks on the UCSC Genome Browser. Peaks were assigned to genes if a) the peak was in a promoter according to MPromDB (Gupta et al., 2011), or b) if the peak was not in a promoter but intragenic, or c) if the peak was neither in a promoter or intragenic but intergenic within 50 kb from the start or end of a gene. Motif discovery was performed using the HOMER program (Heinz et al., 2010). To compute histone acetylation density profiles around the Hlf peaks we used annotatePeaks.pl from Homer (Heinz et al., 2010). Given the bigWig profiles from Lara-Astiaso et al. 2014, we set up Homer to produce the histograms in regions ±1kbp around the center of the peaks of the Hlf ChIP-Seq experiment. We plotted this set of histograms from a given histone experiment together as a heatmap-plot, where each row represents a genomic region around an Hlf peak and the color intensity is proportional to the sequencing library density. Additionally, we plotted the cumulative density around the peaks' center on top. For convenience, we sorted the heatmaps according to Hlf peak height. The script to produce the histograms (bw2histogram.sh, Linux-bash) and to plot heatmaps (HistoneMap MATLAB) can be found at: https://github.com/mscastillo/ChIP-Seq. The naming convention used in Figure 5B is Factor_cell type/line_CL (cell line)/PC (primary cells) and the heatmap was

generated using tools and data available on http://codex.stemcells.cam.ac.uk (Sánchez-Castillo et al., 2015). The generated ChIP-seq data is available on GEO under accession number GSE69817.

RNA-seq

Duplicate cultures of WT GMLPs, transduced overnight on retronectin coated plates with pHAGE2-Hlf/Hlf-IRES-ZsGreen or a pHAGE2 control virus, and Hlf inducible GMLPs maintained in the presence or absence of DOX, were cultured on OP9 stroma in B/NK cell permissive conditions for 4 days. After 4 days of coculture, $ZsGreen^{+}/CD45^{+}$ cells were sorted directly into RLT lysis buffer (1,000 – 50,000 cells). Following initial qualitative assessments using a Bioanalyzer (Agilent Technologies), the samples were subjected to library preparation (SMARTer Ultra Low Input RNA Kit for Sequencing, Clontech) and RNA-seq analysis using an Illumina HiSeq 2500 platform by the Genome Access Technology Center (GTAC, Washington University School of Medicine, St. Louis, MO). The data was next processed according to the GTAC RNA-seq analysis pipeline: sequence reads were mapped to the mouse genome (Ensemble version R72) using Tophat v2.0.8 (Trapnell et al., 2009) with Bowtie2 v2.1.0 (Langmead and Salzberg, 2012). Reads within exons were counted using HTSeq (Anders et al., 2015), and differentially expressed genes were identified using edgeR (Robinson et al., 2010) using the protocol described in the edgeR vignette, and called differential if the FDR was less than 0.05. The RNA-seq data is available in GEO under the accession number GSE69858.

Luciferase assays

To generate the vectors used for the luciferase assay, a 1kb region including the Nfic binding peak and located approximately 6.5kb downstream of the Nfic TSS (GRCm38.p5; Chr10:81413190-81414253), was cloned in the pGL2 vector followed by a SV40 promoter sequence upstream of the firefly luciferase reporter gene (= +6.5kb). The same procedure was used for a shorter 204bp region (GRCm38.p5; Chr10:81413934-81414137) which contains the three candidate HLF binding sites (= Min). As an additional control, an empty pGL2 vector was used. 10,000 Hlf inducible ES cells per sample were seeded onto irradiated MEFs in 48-well plates in complete media without antibiotics (DMEM, FCS 15%, NEAA 1x, Sodium pyruvate 1mM, b-mercaptoethanol 0,1mM and Leukemia Inhibitory Factor 10^{6} units/ml) in the absence or presence of doxycycline (1ug/ml). Each well was co-transfected using Lipofectamine LTX reagent (Invitrogen) with 180ng of each corresponding vector and 20ng of the pRL-TK vector containing the Renilla luciferase reporter gene. 24h after transfection, the luciferase reporter assay was performed using the Dual-Luciferase Reporter Assay System kit (Promega) according to the manufacturer's instructions.

RESOURCE TABLE

REAGENT or RESOURCE	SOURCE	IDENTIFIER
Antibodies		
anti-FLAG	Sigma-Aldrich	Cat#F3165
B220	Biolegend	Clone: RA3-6B2
c-Kit	eBioscience	Clone: 2B8
CD105	Biolegend	Clone: MJ7/18
CD11b	Biolegend	Clone: M1/70
CD150	Biolegend	Clone: TC15-12F12.2
CD16/32	eBioscience	Clone: 93
CD19	Biolegend	Clone: 1D3
CD21	Biolegend	Clone: 7E9
CD24	Biolegend	Clone: M1/69
CD25	BD Pharmingen	Clone: 7D4
CD25	eBioscience	Clone: PC61.5
CD3ε	Biolegend	Clone: 17A2
CD4	Biolegend	Clone: GK1.5
CD41	BD Pharmingen	Clone: MWReg30
CD41	Biolegend	Clone: MWReg30
CD45.1	Biolegend	Clone: A20
CD45.2	Biolegend	Clone: 104
CD48	Biolegend	Clone: HM48-1
CD5	Biolegend	Clone: 53-7.3
CD8a	Biolegend	Clone: 53-7.6
CD8a	Biolegend	Clone: 53-6.7
Flt3	eBioscience	Clone: A2F10
Gr-1	Biolegend	Clone: RB6-8C5
IgD	Biolegend	Clone: 11-26c.2a
IgM	Biolegend	Clone: RMM-1

IL-7Rα	eBioscience	Clone: A7R34
Ly-6D	Sigma-Aldrich	Clone: RGRSL114.8.1
NK1.1	Biolegend	Clone: PK136
Sca1	Biolegend	Clone: D7
Ter-119	Biolegend	Clone: TER-119
Chemicals, Peptides, and Recombinant Proteins		
Annexin V – Cy5	BD Pharmingen	Cat#559933
BamHI	New England Biolabs	Cat#R0136S
Doxycycline food pellets (2g/kg)	Ssniff Specialdiäten	Cat#A112D72003
Doxycycline hyclate	Sigma-Aldrich	Cat#D9891-5G
EcoRI	New England Biolabs	Cat#R0101S
Formaldehyde	Sigma-Aldrich	Cat#F8775
Flt3L	PeproTech	Cat#300-19
IL-2	PeproTech	Cat#212-12
IL-3	PeproTech	Cat#213-13
IL-7	PeproTech	Cat#200-07
IL-15	PeproTech	Cat#210-15
M-CSF	PeproTech	Cat#315-02
NcoI	New England Biolabs	Cat#R0193S
NotI	New England Biolabs	Cat#R0189S
Propidium Iodide	Invitrogen	Cat#P3566
Retronectin	Takara	Cat#T100B
SCF	PeproTech	Cat#250-03
XhoI	New England Biolabs	Cat#R0146S
Critical Commercial Assays		
Anti-biotin Microbeads	Miltenyi Biotec	Cat#130-090-485
Dual-Luciferase Reporter Assay System kit	Promega	Cat#E1910

Gibson Assembly Cloning Kit	New England Biolabs	Cat#E5510S
Q5 High-Fidelity DNA Polymerase	New England Biolabs	Cat#M0491S
KAPA Hifi Hotstart Ready Mix	KAPA Biosystems	Cat#KK2601
KAPA Universal Library Quantification Kit	KAPA Biosystems	Cat#KK4824
Lipofectamine LTX	Invitrogen	Cat#15338100
RNeasy Micro Kit	Qiagen	Cat#74004
SMARTer Ultra Low Input RNA Kit for Sequencing	Clontech	Cat#634888
Ssofast EvaGreen Supermix with Low ROX	Biorad	Cat#1725212
Superscript II Reverse Transcriptase	Invitrogen	Cat#18064014
Superscript III Reverse Transcriptase	Invitrogen	Cat#18080093
SYBR GreenER qPCR SuperMix	Invitrogen	Cat#11762500
T4 DNA ligase	New England Biolabs	Cat#M0202S
Taq DNA polymerase	VWR	Cat#N224-500U
TOPO TA Cloning Kit	Invitrogen	Cat#K4500J10
TruSeq ChIP Library Preparation Kit	Illumina	Cat#IP-202-1012
Deposited Data		
ChIP-seq raw data	NCBI GEO	Accession number: GSE69817
ChIP-seq UCSC track to visualize our data along with that from Lara-Astiaso et al., 2014	NCBI GEO	(http://genome-euro.ucsc.edu/cgi-bin/hgTracks?hgS_doOtherUser=submit&hgS_otherUserName=promufa&hgS_otherUserSessionName=Lund_160719
RNA-seq raw data	NCBI GEO	Accession number: GSE69858
Experimental Models: Cell Lines		
Dox-inducible Hlf KH2 ES cells	This paper	N/A
KH2 ES cells	(Beard et al., 2006)	N/A

OP9 stromal cells	(Kodama et al., 1994)	N/A
OP9-DL1 stromal cells	(Schmitt and Zúñiga-Pflücker, 2002)	N/A
Plat-E cells	Cell Biolabs	Cat#RV-101
Lenti-X 293T cells	Clontech	Cat#632180
Experimental Models: Organisms/Strains		
Mouse: Dox-inducible Hlf mice	This paper	N/A
Oligonucleotides		
KH2 ES cells genotyping primers: Col1a1 fw: tccctcacttctcatccagatatt	Integrated DNA Technologies	(Jaako et al., 2011)
KH2 ES cells genotyping primers: Col1a1 WT rev: agtcttggatactccgtgaccata	Integrated DNA Technologies	(Jaako et al., 2011)
KH2 ES cells genotyping primers: Col1a1 Hlf rev: ggacaggataagtatgacatcatcaa	Integrated DNA Technologies	(Jaako et al., 2011)
KH2 ES cells genotyping primers: Rosa26 fw: aaagtcgctctgagttgttat	Integrated DNA Technologies	(Jaako et al., 2011)
KH2 ES cells genotyping primers: Rosa26 WT rev: ggagcgggagaaatggatatg	Integrated DNA Technologies	(Jaako et al., 2011)
KH2 ES cells genotyping primers: Rosa26 M2rtTA rev: gcgaagagtttgtcctcaacc	Integrated DNA Technologies	(Jaako et al., 2011)
pHAGE2 Hlf/Hlf assembly Fragment 1 Fw: caggtgtcgtgaagcatcacgATGGAGAAAATGTCCCGACAGCTCCCC	Integrated DNA Technologies	Own design
pHAGE2 Hlf/Hlf assembly Fragment 1 Rev: ccagtcccCAGGGGCCCGTGCCTGGC	Integrated DNA Technologies	Own design

pHAGE2 Hlf/Hlf assembly Fragment 2 Fw: ggcccctggggactggtggaggctcaggtggaggctcaggtggaggctcaggtggaggctcaggtggaggcactATGGAGAAAATGTCCCGACAGC	Integrated DNA Technologies	Own design
pHAGE2 Hlf/Hlf assembly Fragment 2 Rev: taggggggggggaggTTACAGGGGCCCGTGCCT	Integrated DNA Technologies	Own design
pHAGE2 Hlf/Dbp assembly Fragment 1 Fw: caggtgtcgtgaagcatcacgATGGAGAAAATGTCCCGACAGCTCCCC	Integrated DNA Technologies	Own design
pHAGE2 Hlf/Dbp assembly Fragment 1 Rev: ccagtcccCAGGGGCCCGTGCCTGGC	Integrated DNA Technologies	Own design
pHAGE2 Hlf/Dbp assembly Fragment 2 Fw: ggcccctggggactggtggaggctcaggtggaggctcaggtggaggctcaggtggaggctcaggtggaggcactATGGCGCGGCCTCTGAGC	Integrated DNA Technologies	Own design
pHAGE2 Hlf/Dbp assembly Fragment 2 Rev: taggggggggggaggTCACAGTGTCCCATGCTGGG	Integrated DNA Technologies	Own design
pHAGE2 Hlf/Tef assembly Fragment 1 Fw: caggtgtcgtgaagcatcacgATGGAGAAAATGTCCCGACAGCTCCCC	Integrated DNA Technologies	Own design

pHAGE2 Hlf/Tef assembly Fragment 1 Rev: ccagtcccCAGGGGCCCGTGCC TGGC	Integrated DNA Technologies	Own design
pHAGE2 Hlf/Tef assembly Fragment 2 Fw: ggcccctggggactggtggaggctcaggt ggaggctcaggtggaggctcaggtggag gctcaggtggaggcactATGTCCGA CGCGGGCGGC	Integrated DNA Technologies	Own design
pHAGE2 Hlf/Tef assembly Fragment 2 Rev: taggggggggggaggTTACAAGGG CCCGTACTTGGTCTCG	Integrated DNA Technologies	Own design
pHAGE2 Hlf/Nfil3 assembly Fragment 1 Fw: caggtgtcgtgaagcatcacgATGGAG AAAATGTCCCGACAGCTCCC C	Integrated DNA Technologies	Own design
pHAGE2 Hlf/Nfil3 assembly Fragment 1 Rev: ccagtcccCAGGGGCCCGTGCC TGGC	Integrated DNA Technologies	Own design
pHAGE2 Hlf/Nfil3 assembly Fragment 2 Fw: ggcccctggggactggtggaggctcaggt ggaggctcaggtggaggctcaggtggag gctcaggtggaggcactATGCAGCT GAGAAAAATGC	Integrated DNA Technologies	Own design
pHAGE2 Hlf/Nfil3 assembly Fragment 2 Rev: taggggggggggaggTTACCTGGA GTCCGAAGC	Integrated DNA Technologies	Own design

pHAGE2 HA-Hlf assembly Fw: caggtgtcgtgaagcatcacgatgtaccca tacgatgttccagattacgctGAGAAAA TGTCCCGACAGCTCC	Integrated DNA Technologies	Own design
pHAGE2 HA-Hlf assembly Rev: taggggggggggaggTTACAGGGG CCCGTGCCT	Integrated DNA Technologies	Own design
pHAGE2 Nfil3 cloning Fw: tagtgcggccgcATGCAGCTGAGA AAAATGCAG	Integrated DNA Technologies	Own design
pHAGE2 Nfil3 cloning Rev: tagtggatccTTACCTGGAGTCCG AAGCC	Integrated DNA Technologies	Own design
pHAGE2 3x FLAG-M33-Hlf assembly fragment 1 Fw: caggtgtcgtgaagcatcacgatgGCAG AGCAGCAGAGAGGG	Integrated DNA Technologies	Own design
pHAGE2 3x FLAG-M33-Hlf assembly fragment 1 Rev: cattttctcATAATGCCTCAAGTTG AAGAAGCC	Integrated DNA Technologies	Own design
pHAGE2 3x FLAG-M33-Hlf assembly fragment 2 Fw: aggcattatGAGAAAATGTCCCGA CAGCTCC	Integrated DNA Technologies	Own design
pHAGE2 3x FLAG-M33-Hlf assembly fragment 2 Rev: taggggggggggaggTTACAGGGG CCCGTGCCT	Integrated DNA Technologies	Own design

pHAGE2 3x FLAG-Hlf/Hlf fragment 1 assembly Fw: caggtgtcgtgaagcatcacgatggactac aaagaccatgacggtgattataaagatcat gatatcgattacaaggatgacgatgacaa gGAGAAAATGTCCCGACAGCT CCCCTTG	Integrated DNA Technologies	Own design
pHAGE2 3x FLAG-Hlf/Hlf assembly fragment 1 Rev: ccagtcccCAGGGGCCCGTGCC TGGC	Integrated DNA Technologies	Own design
pHAGE2 3x FLAG-Hlf/Hlf fragment 2 assembly Fw: ggcccctggggactggtggaggctcaggt ggaggctcaggtggaggctcaggtggag gctcaggtggaggcactATGGAGAA AATGTCCCGACAGC	Integrated DNA Technologies	Own design
pHAGE2 3x FLAG-Hlf/Hlf assembly fragment 2 Rev: taggggggggggaggTTACAGGGG CCCGTGCCT	Integrated DNA Technologies	Own design
MigR1 Hlf assembly Fw: gccggaattagatctcatcacgATGGA GAAAATGTCCCGACAGC	Integrated DNA Technologies	Own design
MigR1 Hlf assembly Rev: agggggggggggcggTTACAGGG GCCCGTGCCT	Integrated DNA Technologies	Own design
pMX 3x FLAG-Hlf/Hlf assembly Fw: tccaccggtcgccaccatggATCACGA TGGACTACAAAG	Integrated DNA Technologies	Own design
pMX 3x FLAG-Hlf/Hlf assembly Fw: tccaccggtcgccaccatggATCACGA TGGACTACAAAG	Integrated DNA Technologies	Own design

pMX 3x FLAG-Hlf/Hlf assembly Rev: ctcgcccttgctcaccatggTGTGGCC ATATTATCATCG	Integrated DNA Technologies	Own design
MigR1 3x FLAG-M33-Hlf assembly Fw: gccggaattagatctcATCACGATGG ACTACAAAGACCATGAC	Integrated DNA Technologies	Own design
MigR1 3x FLAG-M33-Hlf assembly Rev: agggggggggggcggTTACAGGG GCCCGTGCCT	Integrated DNA Technologies	Own design
MigR1 Cebpb assembly Fw: gccggaattagatctcATGCACCGC CTGCTGGCC	Integrated DNA Technologies	Own design
MigR1 Cebpb assembly Rev: agggggggggggcggCTAGCAGTG GCCCGCCGAG	Integrated DNA Technologies	Own design
MigR1 Als2 assembly Fw: tctctaggcgccggaattagatctccaccA TGGACTCAAAGAAGAAAAGC	Integrated DNA Technologies	Own design
MigR1 Als2 assembly Rev: cagtaacgttagggggggggggcggCT AGTTAAGCTTCTCCCG	Integrated DNA Technologies	Own design
MigR1 Ctnna1 assembly Fw: aggcgccggaattagatctccaccATGA CTGCCGTCCACGCA	Integrated DNA Technologies	Own design
MigR1 Ctnna1 assembly Rev: acgttagggggggggggcggTCAGAT GCTGTCCATGGCTTTG	Integrated DNA Technologies	Own design

MigR1 Eps8 assembly Fw: aggcgccggaattagatctccaccATGA ATGGTCATATGTCTAACCGC	Integrated DNA Technologies	Own design
MigR1 Eps8 assembly Rev: acgttagggggggggggcggTCAGTG GCTGCTCCCTTC	Integrated DNA Technologies	Own design
MigR1 Gas6 assembly Fw: aggcgccggaattagatctccaccATGC CGCCACCGCCCGGG	Integrated DNA Technologies	Own design
MigR1 Gas6 assembly Rev: acgttagggggggggggcggCTAGG GGGTGGCATGCTCCACAGG	Integrated DNA Technologies	Own design
MigR1 Gcnt2 assembly Fw: aggcgccggaattagatctccaccATGG GCTCTTGGAAGTAC	Integrated DNA Technologies	Own design
MigR1 Gcnt2 assembly Rev: acgttagggggggggggcggTCAGAA ATACCAGCTCGG	Integrated DNA Technologies	Own design
MigR1 Hip1 assembly Fw: aggcgccggaattagatctccaccATGG ACCGAATGGCCAGC	Integrated DNA Technologies	Own design
MigR1 Hip1 assembly Rev: acgttagggggggggggcggCTACTC TTTGTCCGGTATTGCTTC	Integrated DNA Technologies	Own design
MigR1 Il15 assembly Fw: aggcgccggaattagatctccaccATGA AAATTTTGAAACCATATATGA G	Integrated DNA Technologies	Own design

MigR1 Il15 assembly Rev: acgttagggggggggggcggTCAGG ACGTGTTGATGAAC	Integrated DNA Technologies	Own design
MigR1 Lpl assembly Fw: aggcgccggaattagatctccaccATGG AGAGCAAAGCCCTG	Integrated DNA Technologies	Own design
MigR1 Lpl assembly Rev: acgttagggggggggggcggTCAGC CAGACTTCTTCAG	Integrated DNA Technologies	Own design
MigR1 Nedd4 assembly Fw: tctctaggcgccggaattagatctccaccA TGAGCTCGGACATGGCA	Integrated DNA Technologies	Own design
MigR1 Nedd4 assembly Rev: cagtaacgttagggggggggggcggCT AATCAACGCCATCAAAGC	Integrated DNA Technologies	Own design
MigR1 Nfic assembly Fw: aggcgccggaattagatctccaccATGT ATTCCTCCCCGCTC	Integrated DNA Technologies	Own design
MigR1 Nfic assembly Rev: acgttagggggggggggcggCTAATC CCACAAAGGGAC	Integrated DNA Technologies	Own design
MigR1 Sdc1 assembly Fw: aggcgccggaattagatctccaccATGA GACGCGCGGCGCTC	Integrated DNA Technologies	Own design
MigR1 Sdc1 assembly Rev: acgttagggggggggggcggTCAGG CGTAGAACTCCTCCTGC	Integrated DNA Technologies	Own design

MigR1 Stom assembly Fw: aggcgccggaattagatctccaccATGT CTGACAAACGGCAG	Integrated DNA Technologies	Own design
MigR1 Stom assembly Rev: acgttagggggggggggcggTCAGTG ATTAGAACCCATG	Integrated DNA Technologies	Own design
MigR1 Mgst2 assembly Fw: aggcgccggaattagatctccaccATGG CCGGGGATTCAAGC	Integrated DNA Technologies	Own design
MigR1 Mgst2 assembly Rev: acgttagggggggggggcggTTAGAA GGGCTTCCTCAGTTTC	Integrated DNA Technologies	Own design
MigR1 Sh2d2a assembly Fw: aggcgccggaattagatctccaccATGG AGTTCTGCTTGGCCC	Integrated DNA Technologies	Own design
MigR1 Sh2d2a assembly Rev: acgttagggggggggggcggTCAGG AGGGGCTCCCTCT	Integrated DNA Technologies	Own design
MigR1 St6gal1 assembly Fw: aggcgccggaattagatctccaccATGA TTCATACCAACTTGAAGAG	Integrated DNA Technologies	Own design
MigR1 St6gal1 assembly Rev: acgttagggggggggggcggTCAACA GCGATTGTTCCG	Integrated DNA Technologies	Own design
qRT-PCR primer: Actb fw: CCACAGCTGAGAGGCAAATC	Integrated DNA Technologies	Own design
qRT-PCR primer: Actb rev: CTTCTCCAGGGAGGAAGAGG	Integrated DNA Technologies	Own design

qRT-PCR primer: Ccnb1 fw: AAGGTGCCTGTGTGTGAACC	Integrated DNA Technologies	Own design
qRT-PCR primer: Ccnb1 rev: GTCAGCCCCATCATCTGCG	Integrated DNA Technologies	Own design
qRT-PCR primer: Cfp fw: GAATGTGGCTCCTGGAACTC	Integrated DNA Technologies	Own design
qRT-PCR primer: Cfp rev: TTTGGAGCATGTGACAGAGC	Integrated DNA Technologies	Own design
qRT-PCR primer: Dntt fw: GCCATCCGTGTAGATCTGGT	Integrated DNA Technologies	Own design
qRT-PCR primer: Dntt rev: GCCGCAAGTCTCTCTCAAAC	Integrated DNA Technologies	Own design
qRT-PCR primer: Ebf1 fw: AGCTGCCAACTCACCCTATG	Integrated DNA Technologies	Own design
qRT-PCR primer: Ebf1 rev: CACTGCTGAGACCATGTTGG	Integrated DNA Technologies	Own design
qRT-PCR primer: Erg fw: CAGTAGCCGCCTTGCTAATC	Integrated DNA Technologies	Own design
qRT-PCR primer: Erg rev: TGATGCAGTTGGAGTTGGAG	Integrated DNA Technologies	Own design
qRT-PCR primer: Flt3 fw: TTCCTGCCTCTGGGTCTTTA	Integrated DNA Technologies	Own design
qRT-PCR primer: Flt3 rev: CTGGGTCTCTGTCACGTTCA	Integrated DNA Technologies	Own design
qRT-PCR primer: Hlf fw: GACCCACCTTATGGGACAAA	Integrated DNA Technologies	Own design
qRT-PCR primer: Hlf rev: GGATGCCATTCTCTGACAGG	Integrated DNA Technologies	Own design
qRT-PCR primer: Icosl fw: AGTTCACATGCCGGGTATT	Integrated DNA Technologies	Own design
qRT-PCR primer: Icosl rev: TCAGAGGTGCTGATGACAGG	Integrated DNA Technologies	Own design
qRT-PCR primer: Ikzf3 fw: TACAACCGACTGTGGAGCTG	Integrated DNA Technologies	Own design

qRT-PCR primer: Ikzf3 rev: GAGGTTTGGGCAAGCTGTAG	Integrated DNA Technologies	Own design
qRT-PCR primer: Lambda5 fw: CCATCTAAGCCCCAGTTTTG	Integrated DNA Technologies	Own design
qRT-PCR primer: Lambda5 rev: GGAAGGCAGGAACAGAGTGA	Integrated DNA Technologies	Own design
qRT-PCR primer: Lef1 fw: ACGACAAGGCCAGAGAACAC	Integrated DNA Technologies	Own design
qRT-PCR primer: Lef1 rev: TGTACGGGTCGCTGTTCATA	Integrated DNA Technologies	Own design
qRT-PCR primer: Lgr5 fw: CCCAATGCGTTTTCTACGTT	Integrated DNA Technologies	Own design
qRT-PCR primer: Lgr5 rev: AGGCTCGGTTCCCTGTTAAT	Integrated DNA Technologies	Own design
qRT-PCR primer: Pax5 fw: GGGAGACCTGTTCACACAGC	Integrated DNA Technologies	Own design
qRT-PCR primer: Pax5 rev: CCATGGCTGAATACTCTGTGG	Integrated DNA Technologies	Own design
qRT-PCR primer: Rag1 fw: CTCTCAGGGAGCTCATGGAC	Integrated DNA Technologies	Own design
qRT-PCR primer: Rag1 rev: CGAAACGCTGTGAGTTGAAA	Integrated DNA Technologies	Own design
qRT-PCR primer: Vpreb3 fw: CCTGCCTCTGCTCCTGATAG	Integrated DNA Technologies	Own design
qRT-PCR primer: Vpreb3 rev: CAGCTGAGATGAGCGTCTTG	Integrated DNA Technologies	Own design
Recombinant DNA		
MigR1	(Pear et al., 1998)	N/A
pBS31 targeting vector	(Beard et al., 2006)	N/A
pHAGE2	(Mostoslavsky et al., 2005)	N/A
pMX-GFP	Cell Biolabs	Cat#RTV-050

Forced dimer linker sequence (GGGACTGGTGGAGGCTCAGGTG GAGGCTCAGGTGGAGGCTCAGG TGGAGGCTCAGGTGGAGGCACT)	(Neuhold and Wold, 1993)	N/A
pYX-Asc-Hlf	K.K. DNAFORM	Clone: MGC:76396
Lentiviral construct Hlf/Hlf	This paper	pHAGE2 Hlf/Hlf
Lentiviral construct Hlf/Dbp	This paper	pHAGE2 Hlf/Dbp
Lentiviral construct Hlf/Tef	This paper	pHAGE2 Hlf/Tef
Lentiviral construct Hlf/Nfil3	This paper	pHAGE2 Hlf/Nfil3
Lentiviral construct Hlf	This paper	pHAGE2 HA-Hlf
Lentiviral construct Nfil3	This paper	pHAGE2 Nfil3
Lentiviral construct M33-Hlf	This paper	pHAGE2 M33-Hlf
Lentiviral construct 3x FLAG-Hlf/Hlf	This paper	pHAGE2 3x FLAG-Hlf/Hlf
Retroviral construct Hlf	This paper	MigR1 Hlf
Retroviral construct 3x FLAG-Hlf/Hlf	This paper	pMX 3x FLAG-Hlf/Hlf
Retroviral construct M33-Hlf	This paper	MigR1 3x FLAG-M33-Hlf
Retroviral construct Cebpb	This paper	MigR1 Cebpb
Retroviral construct Als2	This paper	MigR1 Als2
Retroviral construct Ctnna1	This paper	MigR1 Ctnna1
Retroviral construct Eps8	This paper	MigR1 Eps8
Retroviral construct Gas6	This paper	MigR1 Gas6
Retroviral construct Gcnt2	This paper	MigR1 Gcnt2
Retroviral construct Hip1	This paper	MigR1 Hip1
Retroviral construct Il15	This paper	MigR1 Il15
Retroviral construct Lpl	This paper	MigR1 Lpl
Retroviral construct Nedd4	This paper	MigR1 Nedd4
Retroviral construct Nfic	This paper	MigR1 Nfic
Retroviral construct Sdc1	This paper	MigR1 Sdc1
Retroviral construct Stom	This paper	MigR1 Stom
Retroviral construct Mgst2	This paper	MigR1 Mgst2

Retroviral construct Sh2d2a	This paper	MigR1 Sh2d2a
Retroviral construct St6gal1	This paper	MigR1 St6gal1
pGL2 Nfic +6.5kb	This paper	pGL2 Nfic +6.5kb
pGL2 Nfic Min	This paper	pGL2 Nfic Min
Software and Algorithms		
Bowtie2	(Langmead and Salzberg, 2012)	http://bowtie-bio.sourceforge.net/bowtie2/index.shtml
dChip	(Li and Hung Wong, 2001)	https://sites.google.com/site/dchipsoft/
edgeR	(Robinson et al., 2010)	
GEN-E		http://www.broadinstitute.org/cancer/software/GENE-E/index.html
Genome Reference Consortium Mouse Build 38 - mm10	Genome Reference Consortium	http://www.ncbi.nlm.nih.gov/projects/genome/assembly/grc/mouse/
HistoneMap MATLAB		https://github.com/mscastillo/ChIP-Seq
HOMER	(Heinz et al., 2010)	http://homer.ucsd.edu/homer/
HTSeq	(Anders et al., 2015)	
MACS2	(Zhang et al., 2008)	https://github.com/taoliu/MACS/
MPromDB	(Gupta et al., 2011)	http://bioinformatics.wistar.upenn.edu/MPromDb/
Venny	(Oliveros, 2007-2015)	http://bioinfogp.cnb.csic.es/tools/venny/

SUPPLEMENTAL REFERENCES

Anders, S., Pyl, P.T., and Huber, W. (2015). HTSeq--a Python framework to work with high-throughput sequencing data. Bioinformatics *31*, 166-169.

Argiropoulos, B., Yung, E., Xiang, P., Lo, C.Y., Kuchenbauer, F., Palmqvist, L., Reindl, C., Heuser, M., Sekulovic, S., Rosten, P.*, et al.* (2010). Linkage of the potent leukemogenic activity of Meis1 to cell-cycle entry and transcriptional regulation of cyclin D3. Blood *115*, 4071-4082.

Beard, C., Hochedlinger, K., Plath, K., Wutz, A., and Jaenisch, R. (2006). Efficient method to generate single-copy transgenic mice by site-specific integration in embryonic stem cells. Genesis *44*, 23-28.

Bolstad, B.M., Irizarry, R.A., Astrand, M., and Speed, T.P. (2003). A comparison of normalization methods for high density oligonucleotide array data based on variance and bias. Bioinformatics *19*, 185-193.

Gupta, R., Bhattacharyya, A., Agosto-Perez, F.J., Wickramasinghe, P., and Davuluri, R.V. (2011). MPromDb update 2010: an integrated resource for annotation and visualization of mammalian gene promoters and ChIP-seq experimental data. Nucleic Acids Res *39*, D92-97.

Heinz, S., Benner, C., Spann, N., Bertolino, E., Lin, Y.C., Laslo, P., Cheng, J.X., Murre, C., Singh, H., and Glass, C.K. (2010). Simple combinations of lineage-determining transcription factors prime cis-regulatory elements required for macrophage and B cell identities. Mol Cell *38*, 576-589.

Inlay, M.A., Bhattacharya, D., Sahoo, D., Serwold, T., Seita, J., Karsunky, H., Plevritis, S.K., Dill, D.L., and Weissman, I.L. (2009). Ly6d marks the earliest stage of B-cell specification and identifies the branchpoint between B-cell and T-cell development. Genes Dev *23*, 2376-2381.

Jaako, P., Flygare, J., Olsson, K., Quere, R., Ehinger, M., Henson, A., Ellis, S., Schambach, A., Baum, C., Richter, J.*, et al.* (2011). Mice with ribosomal protein S19 deficiency develop bone marrow failure and symptoms like patients with Diamond-Blackfan anemia. Blood *118*, 6087-6096.

Kodama, H., Nose, M., Niida, S., and Nishikawa, S. (1994). Involvement of the c-kit receptor in the adhesion of hematopoietic stem cells to stromal cells. Exp Hematol *22*, 979-984.

Langmead, B., and Salzberg, S.L. (2012). Fast gapped-read alignment with Bowtie 2. Nat Methods *9*, 357-359.

Li, C., and Hung Wong, W. (2001). Model-based analysis of oligonucleotide arrays: model validation, design issues and standard error application. Genome Biol *2*, RESEARCH0032.

Mostoslavsky, G., Kotton, D.N., Fabian, A.J., Gray, J.T., Lee, J.S., and Mulligan, R.C. (2005). Efficiency of transduction of highly purified murine hematopoietic stem cells by lentiviral and oncoretroviral vectors under conditions of minimal in vitro manipulation. Mol Ther *11*, 932-940.

Neuhold, L.A., and Wold, B. (1993). HLH forced dimers: tethering MyoD to E47 generates a dominant positive myogenic factor insulated from negative regulation by Id. Cell *74*, 1033-1042.

Norddahl, G.L., Pronk, C.J., Wahlestedt, M., Sten, G., Nygren, J.M., Ugale, A., Sigvardsson, M., and Bryder, D. (2011). Accumulating mitochondrial DNA mutations drive premature hematopoietic aging phenotypes distinct from physiological stem cell aging. Cell stem cell *8*, 499-510.

Oliveros, J.C. (2007-2015). *Venny. An interactive tool for comparing lists with Venn's diagrams.* http://bioinfogpcnbcsices/tools/venny/indexhtml.

Pear, W.S., Miller, J.P., Xu, L., Pui, J.C., Soffer, B., Quackenbush, R.C., Pendergast, A.M., Bronson, R., Aster, J.C., Scott, M.L.*, et al.* (1998). Efficient and rapid induction of a chronic

myelogenous leukemia-like myeloproliferative disease in mice receiving P210 bcr/abl-transduced bone marrow. Blood *92*, 3780-3792.
Pronk, C.J., and Bryder, D. (2011). Flow cytometry-based identification of immature myeloerythroid development. Methods in molecular biology *699*, 275-293.
Pronk, C.J., Rossi, D.J., Mansson, R., Attema, J.L., Norddahl, G.L., Chan, C.K., Sigvardsson, M., Weissman, I.L., and Bryder, D. (2007). Elucidation of the phenotypic, functional, and molecular topography of a myeloerythroid progenitor cell hierarchy. Cell stem cell *1*, 428-442.
Robinson, M.D., McCarthy, D.J., and Smyth, G.K. (2010). edgeR: a Bioconductor package for differential expression analysis of digital gene expression data. Bioinformatics *26*, 139-140.
Schmitt, T.M., and Zúñiga-Pflücker, J.C. (2002). Induction of T cell development from hematopoietic progenitor cells by delta-like-1 in vitro. Immunity *17*, 749-756.
Sánchez-Castillo, M., Ruau, D., Wilkinson, A.C., Ng, F.S., Hannah, R., Diamanti, E., Lombard, P., Wilson, N.K., and Gottgens, B. (2015). CODEX: a next-generation sequencing experiment database for the haematopoietic and embryonic stem cell communities. Nucleic Acids Res *43*, D1117-1123.
Trapnell, C., Pachter, L., and Salzberg, S.L. (2009). TopHat: discovering splice junctions with RNA-Seq. Bioinformatics *25*, 1105-1111.
Tung, J.W., Parks, D.R., Moore, W.A., and Herzenberg, L.A. (2004). Identification of B-cell subsets: an exposition of 11-color (Hi-D) FACS methods. Methods Mol Biol *271*, 37-58.
Zhang, Y., Liu, T., Meyer, C.A., Eeckhoute, J., Johnson, D.S., Bernstein, B.E., Nusbaum, C., Myers, R.M., Brown, M., Li, W.*, et al.* (2008). Model-based analysis of ChIP-Seq (MACS). Genome Biol *9*, R137.